

# *FUSE* Measurements of Far Ultraviolet Extinction. II. Magellanic Cloud Sight Lines<sup>1</sup>

Stefan I. B. Cartledge<sup>1</sup>, Geoffrey C. Clayton<sup>1</sup>, Karl D. Gordon<sup>2</sup>, Brian L. Rachford<sup>3</sup>, B. T. Draine<sup>4</sup>, P. G. Martin<sup>5</sup>, John S. Mathis<sup>6</sup>, K. A. Misselt<sup>2</sup>, Ulysses J. Sofia<sup>7</sup>, D. C. B. Whittet<sup>8</sup>, and Michael J. Wolff<sup>9</sup>

## ABSTRACT

We present an extinction analysis of nine reddened/comparison star pairs in the Large and Small Magellanic Clouds based on *Far-Ultraviolet Spectroscopic Explorer (FUSE)* FUV observations. To date, just two LMC sight lines have probed dust grain composition and size distributions in the Magellanic Clouds using spectral data for wavelengths as short as 950 Å. We supplement these two with data from 4 regions distinguished by their IR through UV extinction curves and grouped as LMCAvg, LMC2, SMC bar and SMC wing. Despite the distinct characters of extinction in the Clouds and Milky Way, our results are generally analogous to those found for Galactic curves—namely, that the *FUSE* portions of each extinction curve are described reasonably well by Fitzpatrick & Massa curves fitted only to longer wavelength data and lack any dramatic new extinction features, and any deviations from the Cardelli, Clayton, & Mathis (CCM)

---

<sup>1</sup>Department of Physics and Astronomy, Louisiana State University, Baton Rouge, LA 70803; scar-  
tled@lsu.edu, gclayton@fenway.phys.lsu.edu

<sup>2</sup>Steward Observatory, University of Arizona, Tucson, AZ 85721; kgordon@as.arizona.edu, mis-  
selt@as.arizona.edu

<sup>3</sup>Center for Astrophysics and Space Astronomy, Department of Astrophysical and Planetary Sciences,  
University of Colorado at Boulder, Campus Box 389, Boulder, CO 80309-0389; rachford@casa.colorado.edu

<sup>4</sup>Princeton University Observatory, Peyton Hall, Princeton, NJ 08544; draine@astro.princeton.edu

<sup>5</sup>Canadian Institute for Theoretical Astrophysics, University of Toronto, Toronto, Ontario M5S 3H8  
Canada; pgmartin@cita.utoronto.ca

<sup>6</sup>University of Wisconsin-Madison, 475 North Charter Street, Madison, WI 53706; mathis@astro.wisc.edu

<sup>7</sup>Department of Astronomy, Whitman College, Walla Walla, WA 99362; sofiauj@whitman.edu

<sup>8</sup>Department of Physics and Astronomy, Rensselaer Polytechnic Institute, Troy, NY 12180-3590;  
whitted@rpi.edu

<sup>9</sup>Space Science Institute, 3100 Marine Street, Suite A353, Boulder, CO 80303-1058; wolff@colorado.edu

formalism continue into FUV wavelengths. A Maximum Entropy Method analysis of all of these curves suggests that LMC Avg and SMC wing sight lines, whose extinction parameters more closely resemble those for Galactic paths, require more silicon and/or carbon in dust than current abundance measurements would indicate are available. The requirements for LMC2 and SMC bar sight lines do not fully tax the available reservoirs, in part because large grains contribute less to the extinction in these directions. An intermediate product of this extinction analysis is the measurement of new  $\text{H}_2$  abundances in the Magellanic Clouds. Collectively considering Cloud sight lines that possess significant  $\text{H}_2$  column densities,  $E(B-V)/N(\text{H I})$  ratios are reduced by significant factors relative to the Galactic mean, whereas the corresponding  $E(B-V)/N(\text{H}_2)$  values more closely resemble their Galactic counterpart. These trends reflect the fact that among these sight lines  $f(\text{H}_2)$ -values are lower than those common in the Milky Way for paths with similar degrees of reddening.

*Subject headings:* ISM: abundances — ultraviolet: ISM

## 1. Introduction

An important step toward a complete understanding of the formation, structure, and composition of interstellar dust is the study and discrimination of factors that produce changes in the observed wavelength-dependent extinction of stars due to grains. The Large and Small Magellanic Clouds (LMC and SMC, respectively) are metal-poor relative to the Galaxy; recent estimates imply that the LMC and SMC have overall metallicities at levels 0.5 and 0.2–0.25, respectively, of the Galactic ISM (Welty et al. 2001). Dust-to-gas ratios determined for these galaxies, as represented by  $E(B-V)/N(\text{H I})$ , are also reduced (by factors of about 4 and 10; Bouchet et al. 1985; Fitzpatrick 1986), indicating that LMC and SMC dust components and their formation mechanisms are not inconsistent with Galactic components and mechanisms. Nevertheless, there are differences in extinction among these three galaxies.

Early investigations of the extinction properties of Magellanic Cloud dust identified several sight lines that exhibited marked differences from curves produced by grains in the Milky Way (e.g., Nandy et al. 1980; Koornneef & Code 1981; Rocca-Volmerange et al. 1981).

---

<sup>1</sup>Based on observations with the NASA-CNES-CSA *Far-Ultraviolet Spectroscopic Explorer*, which is operated for NASA by the Johns Hopkins University under NASA contract NAS-32985.

It was noted in comparing these curves that the 2175 Å bump strength was reduced in the LMC relative to the Galaxy, and somewhat further diminished for curves characteristic of the SMC. Similarly, the FUV rise evident in LMC and SMC extinction curves is stronger than that common in the Galaxy. Subsequent studies have identified regional variation in Magellanic Cloud curves, associating a distinctive LMC wavelength dependence with the supershell LMC2 (Misselt, Clayton, & Gordon 1999), a steeper UV curve with the star-forming bar region of the SMC, and extinction more closely resembling Galactic curves with other portions of the Clouds. Recently, Gordon et al. (2003) (hereafter G03) completed a comprehensive comparison of Galactic, LMC, and SMC extinction curves from near-infrared to ultraviolet (UV) wavelengths ( $\lambda \gtrsim 1150 \text{ \AA}$  or  $1/\lambda \lesssim 8.7 \mu\text{m}^{-1}$ ); G03 confirmed that curves characteristic of the LMC2 grouping and the SMC bar do not conform to the Cardelli, Clayton, & Mathis (1989) (CCM) parameterization of Galactic extinction based on  $R_V \equiv A(V)/E(B-V)$ .

The strength of their UV extinction is a key feature distinguishing LMC, SMC, and Galactic curves; in particular, the steeper short-wavelength slopes associated with Magellanic Cloud extinction curves can be diagnostic of differences in dust compositions and grain size distributions, given appropriate measures of elemental abundances in their respective interstellar media (Draine 2003). However, the extension of Magellanic Cloud extinction curves into the FUV ( $> 8.7 \mu\text{m}^{-1}$ ) is complicated by the requirement that interstellar H<sub>2</sub> absorption be removed from the spectra before an extinction curve can be produced using the pair method. Previous efforts in this area, even for Milky Way sight lines, have been hampered by a lack of high quality data. In particular, instrumental issues of scattered light, time-variable sensitivity, and a limited sample (both target and comparison objects) restricted the utility of the *Copernicus* dataset (cf. Jenkins et al. 1986; Snow, Allen, & Polidan 1990), the *Voyager* UVS data suffer from low resolution which prevents explicit identification and removal of the molecular hydrogen contribution, and the remaining available data [e.g., rocket - Green et al. 1992; Lewis, Cook, & Chakrabarti 2005; *Hopkins Ultraviolet Telescope (HUT)* - Buss et al. 1994; *Orbiting Retrievable Far and Extreme Ultraviolet Spectrometer (ORFEUS)* - Sasseen et al. 2002] include only a few Galactic sight lines. *Far Ultraviolet Spectroscopic Explorer (FUSE)*, however, has revolutionized our ability to study interstellar molecular hydrogen. Its combination of slightly better spectral resolution and much greater detector sensitivity than *Copernicus* allows H<sub>2</sub> to be detected throughout much larger and more diverse portions of the Galaxy and even in the Magellanic Clouds (Shull et al. 2000; Rachford et al. 2002; Tumlinson et al. 2002). Thus, *FUSE* data are uniquely suited to investigating the FUV extinction properties of Milky Way, LMC, and SMC sight lines and what any differences reveal about the dust populations in each galaxy.

Recently, Clayton et al. (2003) used a modified maximum entropy method (MEM) to

fit extinction components to IR through UV curves for stars both in the Galaxy and in the Clouds; they demonstrated that the average SMC bar extinction curve was best fit using a grain distribution in which small silicate and amorphous carbon grains play a much larger role than in the mean Galactic extinction. However, this result is at odds with Welty et al. (2001), whose data suggested negligible silicon depletion in several gas cloud components along a sight line probing the SMC ISM. In order to address issues such as dust composition, particularly for small grains enhancing FUV extinction in the Clouds, it would be helpful to explore LMC and SMC extinction curves shortward of the UV range that Clayton et al. (2003) were confined to by their *International Ultraviolet Explorer (IUE)* data; unfortunately, FUV extinction curves have been published to date for only very few reddened Magellanic Cloud stars (Clayton et al. 1996; Hutchings & Giasson 2001).

In this paper, we construct new extinction curves for nine pairs of reddened and unreddened LMC and SMC stars by supplementing the IR through UV curves published by G03 with recent *FUSE* observations of 16 Magellanic Cloud targets. The *FUSE* data allow us to extend the Clayton et al. (2003) analysis of dust composition and grain size distribution to FUV wavelengths, where extinction is dominated by small grains and the differences between Galactic and Magellanic Cloud curves are particularly prominent. This is the second in a series of three papers exploring extinction in the FUV. Paper I (Sofia et al. 2005) dealt with a small set of Galactic extinction curves characterized by a broad range of  $R_V$ -values; Paper III (in preparation) will examine a much larger sample of Galactic sight lines in an effort to search rigorously for any trends among observed extinction parameters when FUV data are fully considered.

## 2. Observations and Data Extraction

The present sample of 16 LMC and SMC stars includes all stars in the *FUSE* archive for which the spectral match between the reddened and unreddened stars has been rigorously evaluated and there exist spectral data from IR to UV wavelengths. Each reddened star has previously been studied by G03; we use the same photometry sources and procedures to construct the IR to UV portions of the extinction curves for the pairs adopted in this study, with the exception that early 2MASS photometry has been superseded in our analysis by data from the recent *All Sky Release*. In particular, it should be noted that the  $R_V$  values listed in Table 1, which summarizes the properties of each extinction pair, differ slightly from those published by G03 due to this update of the IR data. Consequently, the values of  $A_V$  and  $N(\text{H I})/A_V$  in the table are also affected. The FUV portions of the extinction curves (shortward of the H I Ly $\alpha$  line) were derived from the new and archival *FUSE* observations

listed in Table 2. All of the raw data were processed using the latest release of CALFUSE (v3.0). The calibrated spectra for each channel were cross-correlated, shifted to a common wavelength scale, and combined based on exposure time in cases where several observations of a star existed. Also, in cases where the different observations or different *FUSE* channels produced conflicting flux levels for a given wavelength (e.g., due to channel misalignment), the data for these observations or channels were linearly adjusted to match the maximum observed flux across the regions of overlap. General details on *FUSE* observations have been published by Sahnou et al. (2000a). We point out here, however, that each observation produces eight spectra nearly 100 Å in length with individual dispersion characteristics. The LiF channel spectra (LiF1A, LiF1B, LiF2A, LiF2B) cover most wavelengths from 990–1190 Å twice over; the spectral region from 910–1110 Å are similarly sampled by the SiC channels (SiC1A, SiC1B, SiC2A, SiC2B). Sample spectra of both poor and fine quality appear in Figure 1, using the data from the reddened star AzV 456 and its comparison star AzV 70, respectively.

## 2.1. Molecular Hydrogen Modelling and Removal

Strong FUV H<sub>2</sub> absorption bands can significantly alter the appearance of stellar spectra, depending upon the column density of molecular gas along the line of sight. Consequently, a molecular hydrogen model was constructed for each sight line using procedures patterned generally after those used by Rachford et al. (2001, 2002). The underlying assumption we made in measuring the interstellar H<sub>2</sub> for each sight line was that the model includes only two velocity components, one corresponding to Milky Way gas and one associated with H<sub>2</sub> in the appropriate Magellanic Cloud. The equivalent width measurements for distinct profiles of each component were entered into separate tables, so that molecular hydrogen measurements could be made individually for each galaxy using a curve-of-growth (CoG) analysis. Unfortunately, the velocity separation of Galactic and Magellanic Cloud components often resulted in blended absorption profiles at several points in a given spectrum. In general, the construction of a reasonable CoG for most of the sight lines required more equivalent width measurements than were available from the unblended and isolated H<sub>2</sub> absorption lines. To remedy this problem, the profile-fitting code FITS6P<sup>2</sup> and IRAF<sup>3</sup> plotting routines were

---

<sup>2</sup>The FITS6P code models absorption profiles based on varying the column densities, *b*-values, and velocities of input interstellar components. More details on the algorithm can be found in Welty, Hobbs, & York (1991).

<sup>3</sup>IRAF is distributed by the National Optical Astronomy Observatories, which are operated by the Association of Universities for Research in Astronomy, Inc., under cooperative agreement with the National

used in conjunction with our IDL<sup>4</sup> code (Rachford et al. 2001, 2002) to deconvolve blended profiles and fill out each CoG with as many measurements as could reliably be made. The CoG analysis, however, was generally limited to  $J \geq 3$  because the  $J \leq 2$  lines were saturated to the extent that they possessed broad damping wings that the equivalent width measurement algorithm could not reliably distinguish from the stellar continuum. Thus, an iterative curve-fitting procedure was an additional requirement so that simultaneous determinations of Galactic and Magellanic Cloud column densities for these lower H<sub>2</sub> rotational excitation levels could be made. The complete molecular hydrogen models, including column densities for the available  $J$  levels, the associated  $b$ -value, and the derived kinetic and excitation temperatures (these last properties are discussed in section 3.1), are summarized in Tables 3 and 4 for all of our LMC and SMC sight lines; Table 3 characterizes the Galactic component for each sight line where one was detected, while Table 4 details the properties of each Magellanic Cloud component.

Once molecular hydrogen absorption models had been constructed, each spectrum was corrected for this absorption. All of the *FUSE* data for each star were combined into a single spectrum by shifting the calibrated channel spectra to a common wavelength reference and averaging the fluxes, weighted by the flux uncertainty at each point in the overlapping regions. Although there are significant differences in the data dispersion properties for each channel, the merged spectrum for each star is of sufficient quality for the construction of a reliable extinction curve. The “worm” problem in *FUSE* data (Sahnow et al. 2000b) was strong only in LiF1B. Its appearance in the data for this detector segment was identified by a comparison with the LiF2A flux as the data for all detector segments were merged into a single spectrum for each sight line; the portions of the LiF1B spectrum contaminated by the worm were eliminated from the merging process. A running cross-correlation of the normalized H<sub>2</sub> absorption profile corrected for any wavelength mismatches, and the full final model was divided into the merged *FUSE* spectrum to complete the “removal” of the molecular hydrogen features. Atomic hydrogen was not measured for each sight line individually, but its signature, specifically the Ly $\alpha$  and Ly $\beta$  lines, was removed after the ratio of the reddened and comparison spectra was calculated as a function of wavelength. Although *FUSE* spectra cover wavelengths from 905 through 1187 Å, data shortward of 1044 Å (our Ly $\beta$  cutoff) were not included in this analysis due to limitations in data quality.

In the interest of consistency in instrument response, *FUSE* flux levels were then man-

---

Science Foundation.

<sup>4</sup>IDL is an acronym for Interactive Data Language, a common programming tool developed by Research Systems, Inc.

ually rescaled to match *IUE* fluxes over the wavelength range common to both instruments (1150 – 1185 Å) when the full IR to FUV spectra were constructed; given recent improvements to the calibration of *IUE* data (Massa & Fitzpatrick 2000), flux errors associated with this instrument have not yet been surpassed by the latest *FUSE* calibration (Sahnou et al. 2000a). Generally, mean fluxes for the data from each instrument agreed to within 20%, although there were a few targets for which the discrepancies exceeded this range. The scalings applied to each *FUSE* spectrum (the ratio of *IUE* to *FUSE* flux in the overlap region) are given in Table 5.

## 2.2. The Extinction Curves

We have constructed extinction curves using the pair method (e.g., Massa, Savage, & Fitzpatrick 1983), normalized to  $A(V)$  through  $R_V$ ; the pairs of reddened and unreddened stars in the LMC and SMC were selected (G03) and are listed in Table 1. In an effort to minimize uncertainties in each extinction curve, particularly from spectral mismatch, a detailed comparison of the *FUSE* spectrum for each star with similarly-typed unreddened candidates was performed, and the extinction pairs matched by G03 using *IUE* were also found to be well-matched in the FUV. Assembly of the extinction curve corresponding to each pair was accomplished using the same procedures and near-infrared through UV data outlined by G03. We have also constructed average extinction curves for the subsets of the current sample associated with the LMCavg and LMC2 regions considered previously in the UV (Misselt, Clayton, & Gordon 1999; G03). Each of the individual LMC curves and the average curves have been fit to the Fitzpatrick & Massa (1990) parameterization; the results are presented in Table 6. The two sight lines in the SMC, one representing each of the bar and wing regions, are considered individually.

A quick examination of the individual Magellanic Cloud extinction curves presented in Figure 2 reveals that the *FUSE* portion of each curve is generally consistent with an extension of the data from longer wavelengths. When the calibrated and  $H_2$ -adjusted fluxes were initially compared, however, slight offsets were apparent between the portions of the curve on either side of the  $Ly\alpha$  line. Comparing the size of the gaps in the Magellanic Cloud data with the Galactic curves studied in Paper I led to the conclusion that the quality of the data for our reddened stars might have compromised the accuracy of the extinction curve construction. In particular, the S/N of the *FUSE* data seemed to be inversely proportional to the size of the offset and there were noticeable flux level differences for some spectra between the *IUE* and the merged *FUSE* data in the spectral overlap region. The Galactic sight lines had much better S/N values, negligible offsets, and good agreement between *IUE*

and *FUSE* fluxes, whereas the Magellanic Cloud data suffered generally poor S/N, noticeable offsets, and sometimes poor flux agreement in the overlap. In order to reduce the offsets, the *FUSE* data for the Cloud sight lines were linearly adjusted (a wavelength-independent multiplicative factor was applied to the flux) over the entire FUV bandpass so that their fluxes matched *IUE* in the instruments’ overlap region. An example of one of the more egregious cases is plotted in Figure 3, including a comparison of the *FUSE* flux levels both before and after adjustment to the *IUE* flux level. The magnitude of each shift was estimated in increments of  $0.05 \times flux_{IUE}$ ; the systematic uncertainty associated with this adjustment has been propagated through all subsequent error calculations. Typically, the shifts improved the appearance of the curves, although the offsets were not eliminated in all cases. Given the general smoothness of the transition between UV and FUV portions of the extinction curve in most cases, it might seem reasonable to introduce further shifts to align these segments; nevertheless, because the observed offsets fall generally within the error bounds, because we are interested in the detailed shape of the curve at UV and FUV wavelengths, and since we have no independent objective basis for such shifts, no further processing of the individual curves has been performed. It should also be noted that any residual offsets appear to be biased in the direction of decreased  $A(\lambda)/A(V)$ ; thus, abundance requirements derived from the FUV data may be slight underestimates.

### 3. Discussion

#### 3.1. H<sub>2</sub> in the Magellanic Clouds

As already mentioned, a notable difficulty in deriving extinction curves that extend into the FUV is the existence of strong molecular hydrogen absorption bands longward of the Ly $\alpha$  line. Nevertheless, stellar observations of sufficient quality to allow the H<sub>2</sub> absorption to be modelled and removed not only permit the construction of an extinction curve but also provide more direct information on the intervening ISM. Recently, Tumlinson et al. (2002) completed a survey of molecular hydrogen in the LMC and SMC using several *FUSE* observations of each Cloud; our sample introduces 15 new sight lines into the mix.

In considering these new molecular hydrogen measurements, however, it should be recognized that the current *FUSE* data generally have much lower signal-to-noise ratios than Galactic observations. In fact, they are also somewhat lower than the values for previously-observed Magellanic Cloud targets. Tumlinson et al. (2002) reported typical  $4\sigma$  equivalent width limits of 30–40 mÅ, a level similar to values of 20–50 mÅ for our comparison stars but much lower than the 50–120 mÅ characteristic of the reddened targets. Because of these data limitations, and because the goal of generating a reliable FUV continuum was given



a somewhat higher priority than making a rigorous assessment of molecular hydrogen, any column densities smaller than about  $10^{17} \text{ cm}^{-2}$ , and a few that are somewhat larger, are subject to sizable uncertainties. Nevertheless, we consider the models listed in Tables 3 and 4 to be reasonable tallies of the  $\text{H}_2$  along each sight line.

In order to more fully understand how the new sight lines mesh with the Tumlinson et al. (2002) Magellanic Cloud  $\text{H}_2$  analysis, we have adopted the atomic hydrogen measurements previously published by Fitzpatrick (1985a,b) for the individual sight lines (see Table 7); for the pair listings in the table, we use the values derived directly from the extinction curves by G03. It should be noted here that the process of determining atomic hydrogen column densities for the Magellanic Clouds is complicated by the large quantities detected along each sight line. The breadth of the  $\text{Ly}\alpha$  absorption profile produced by typical interstellar hydrogen distributions with line-of-sight lengths exceeding even a few kiloparsecs is sufficient to mask distinctions between separate velocity components; in particular, the profiles for atomic hydrogen gas in the LMC or SMC are often inextricably blended with their Galactic counterparts. Tumlinson et al. (2002) dealt with this problem by calibrating 21 cm emission measurements to  $\text{Ly}\alpha$  from the sight lines in their sample for which the Galactic and Magellanic Cloud 1215 Å profiles were not severely blended. Atomic hydrogen column densities for the remaining paths in the data set were then estimated using this calibration and the observed 21 cm emission. G03 assessed Magellanic Cloud H I column densities by measuring the  $\text{Ly}\alpha$  profile in the reddened-to-comparison ratio spectrum for each extinction pair, under the assumption that the Milky Way components would cancel each other. Each of these methods is subject to a significant level of uncertainty; if vertical error bars were to be plotted in Figure 4, among the Magellanic Cloud sight lines they might typically be about 0.3 dex and occasionally larger than 1.0 dex. Nevertheless, differences between the Fitzpatrick (1985a,b) H I values for the individual sight lines in each extinction pair generally are well matched by the corresponding column densities derived by G03.

Considered individually, our LMC and SMC sight lines and those studied by Tumlinson et al. (2002) exhibit similar ranges in characteristics such as the molecular hydrogen fraction  $f(\text{H}_2)$  ( $\equiv 2N(\text{H}_2)/[N(\text{H I}) + 2N(\text{H}_2)]$ ) and the Magellanic Cloud portion of the color excess  $E'(B-V)$ ;<sup>5</sup> values for the two LMC sight lines studied by Gunderson, Clayton, & Green (1998) also match these samples. Since the current dataset was selected for its extinction properties, we cannot speak to the overall frequency of molecular hydrogen detection in the Clouds. However, as shown in Figure 4, the  $f(\text{H}_2)$ -values for paths along which we detect a Cloud-based  $\text{H}_2$  component agree with the levels set by previously observed LMC

---

<sup>5</sup>Following the procedure of Tumlinson et al. (2002), we adopt the definition  $E'(B-V) = E(B-V) - x$ , where  $x$  is 0.075 and 0.037 for LMC and SMC paths, respectively.

and Galactic sight lines of large  $E(B-V)$ . Notably, the sight lines toward AzV 456 and Sk  $-67^\circ 2$  possess larger molecular hydrogen fractions than any examined by Tumlinson et al. (2002); meanwhile, among the paths directed toward our comparison stars we detect no Magellanic  $H_2$  components.

Based on the previously-studied sight lines toward Sk  $-66^\circ 19$  and Sk  $-69^\circ 270$ , it was found that while the gas-to-dust ratio  $N(\text{H I})/E'(B-V)$  is much larger in the Clouds than typically seen in the Milky Way, the quantity  $N(H_2)/E'(B-V)$  has a similar value in each galaxy (Clayton et al. 1996; Gunderson et al. 1998). This suggests a close relationship between dust and  $H_2$ . Similar behavior is evident for our new sight lines, since although the ratios  $N(\text{H I})/E'(B-V)$  for these paths are roughly 4–10 times larger than the Galactic mean, comparing  $H_2$  column densities with the same color excesses leads to a range of values around the Galactic average. In this way our new sight lines complement the paths studied by Gunderson et al. (1998) and the more heavily reddened paths of Tumlinson et al. (2002), implying generally lower values for  $f(H_2)$  in the Clouds; nevertheless, the current dataset includes sight lines with unique properties. Plotting the LMC  $N(\text{H I})/E'(B-V)$  ratio as a function of  $E(B-V)$  (see Figure 5), there is a clear distinction between Sk  $-67^\circ 2$  and other reddened sight lines: this one LMC path is characterized by an “atomic” ratio appropriate to Galactic curves, but because of its large molecular hydrogen column density the total gas-to-dust ratio approaches the values for other LMC sight lines. Coupled with its Milky Way-like  $N(\text{H I})$  ratio, the agreement exhibited between the gas-to-dust ratios for Sk  $-67^\circ 2$ , the sight line with the largest  $f(H_2)$ -value in our sample, and sight lines dominated by atomic gas reinforces the concept that the mechanisms governing dust formation in the Galaxy and LMC are similar and that any differences in extinction arise out of how interstellar environmental conditions are manifested in dust grain population characteristics. The SMC sight line AzV 456 also possesses a “Galactic” value for  $N(\text{H I})/E'(B-V)$  that gives a  $N(\text{H}_{\text{Total}})/E'(B-V)$  ratio more closely resembling the values determined by Tumlinson et al. (2002) for other SMC paths.

Further details of the interstellar conditions, specifically the temperatures  $T_{01}$  and  $T_{ex}$ , in the Clouds can be derived from the relative rotational level populations of the individual sight lines (Table 4). When the cloud density is sufficiently high and  $H_2$  column densities are large enough for the gas to become substantially molecular, ortho-para conversion will bring  $T_{01}$  ( $\equiv \frac{E_1 - E_0}{k} \frac{\log(e)}{\log(N(J=0)/g_0) - \log(N(1)/g_1)} = \frac{170\text{K}}{\ln(9N(0)/N(1))}$ ) close to the kinetic temperature. Except for the AzV 462 sight line, its value is fairly uniform among the LMC and SMC components of our  $H_2$  models and we derive a weighted mean temperature of  $50 \pm 3$  K. The Magellanic Cloud component of  $H_2$  toward AzV 462 has the lowest column density among our extragalactic values, and the assumption that this value is consistent with the kinetic temperature breaks down. The mean temperature we have derived for the Magellanic Cloud

components neglects AzV 462 and is somewhat lower than the overall Galactic mean of  $77\pm 17$  K (Savage et al. 1977), but is consistent with both the value  $55\pm 8$  K derived from the Galactic subsample for which  $N(\text{H}_2) > 20.4$  (Rachford et al. 2002) and temperatures derived by Tumlinson et al. (2002) for Magellanic Cloud gas along sight lines with some of the largest molecular column densities. It should be noted that the errors ascribed to each temperature listed in Tables 3 and 4 were derived from column density uncertainties, which were often large. Thus, kinetic temperatures with uncertainties larger than about 60 K should be regarded as less reliable. In particular, the formal uncertainty is listed in each case, even where it exceeds the calculated temperature, in order to indicate the relative reliability of each determination. We have also determined  $T_{ex}$  for each sight line from the slope in a plot of  $N(J = 2, 3, 4, 5)$  versus the excitation potential.<sup>6</sup> This excitation temperature reflects the influence of fluorescent UV pumping and  $\text{H}_2$  formation in excited states on the molecular hydrogen rotational level population (Jura 1975; Black & Dalgarno 1976). Like  $T_{01}$ , it is fairly uniform among the LMC and SMC sight lines and we calculate a weighted mean of  $244\pm 33$  K, similar to previously-determined values for Magellanic Cloud sight lines (Shull et al. 2000). Comparing the column density ratios  $N(4)/N(2)$  and  $N(5)/N(3)$  for our sample with Figure 11 from Tumlinson et al. (2002), we find that these sight lines are reasonably typical of their high  $N(\text{H}_2)$  paths; consequently, our measurements support their conclusions that the  $\text{H}_2$  formation rate in the Clouds is low (10–40% of Galactic rates) and that at least some regions are illuminated by relatively intense radiation fields (10–100 times the Galactic mean). We note, however, that the proportion of outliers in our sample that do not fit the range of Galactic models calculated by Tumlinson et al. (2002) is much smaller than theirs. Values of  $T_{01}$  and  $T_{ex}$  were also derived for the Galactic components of our  $\text{H}_2$  models. A mean of  $T_{01} = 67\pm 4$  K was derived for the sight lines with larger column densities and more robust measurements, although higher, and likely to be in part non-thermal, temperatures are implied for several of the more diffuse paths. Excitation temperatures for the Galactic components ( $239\pm 38$  K) are similar to those we have determined for the Magellanic Clouds.

### 3.2. FUV Extinction in the Magellanic Clouds

Before *FUSE*, only two reddened sight lines outside the Galaxy had been studied in the FUV (Clayton et al. 1996). Both regional extinction groups in the LMC are represented

---

<sup>6</sup>More generally,  $T_{ex}$  is associated with values of  $T_{J-2,J} \equiv \frac{E_J - E_{J-2}}{k} \frac{\log(e)}{\log[N(J-2)/g_{J-2}] - \log[N(J)/g_J]} = \frac{170\text{K} \times (2J-1)}{\ln[\frac{2J+1}{2J-3} \frac{N(J-2)}{N(J)}]}$  (for  $J \geq 2$ ), the temperature derived from comparing the populations of successive even or odd  $J$  levels.

by these two stars; specifically, Sk -66°19 is associated with LMCAvg and Sk -69°270 with LMC2 (Misselt et al. 1999). The UV extinction curves for these stars are typically non-CCM, but they share the trait of most Galactic curves in that their UV extinction slope blends smoothly into the FUV. These two sight lines have been included for comparison in Table 6, which defines the LMC2 and LMCAvg subsamples, although they were left out of the average extinction curves for those regions. Hutchings & Giasson (2001) published FUV extinction curves for 3 sight lines in each of the LMC and the SMC using *FUSE* data. Unfortunately, the values of  $\Delta(B-V)$  for the reddened/unreddened star pairs chosen for that study are too small ( $\sim 0.02-0.07$  mag) for detailed extinction studies. More specifically, these reddening values are comparable in size to the variation in the foreground  $E(B-V)$  and similar to the magnitude of the photometric uncertainties (Schwering & Israel 1991; Oestreicher, Gochermann, & Schmidt-Kaler 1995; Massey 2002). So, within the uncertainties there is no significant reddening difference for any of the star pairs in Hutchings & Giasson (2001), and those sight lines are not included in this study.

The new LMC and SMC FUV extinction curves presented here seem to follow the trend of Sk -69°270 and Sk -66°19. Despite any small remaining offsets between the *IUE* and *FUSE* extinction curves (see § 2.1), the new FUV curves closely follow an extrapolation of their FM fits from the UV. Out of our sample, only two curves exhibit significant deviations from this overall trend, AzV 456 and Sk -69°228. AzV 456 is our lone reddened star situated in the SMC wing, and the *FUSE* portion of its extinction curve more closely resembles its FUV CCM curve than an extrapolation of its FM fit in the UV. Coincidentally, the disagreement with the FM fit begins near the onset of molecular hydrogen absorption features; however, attempting to reconcile the two portions of the *FUSE* curve by adjusting the H<sub>2</sub> column densities indicates that a single component for the Clouds cannot reproduce the observed continuum level shift, nor does it appear that a simple combination of overlapping components would accomplish this result. The effect does not appear to be related to a difference in the sensitivity of the various *FUSE* channels either, since the continuum across this spectral region is contained in both the LiF1B and LiF2A detector bands. Similar kinks are apparent to a much smaller degree in the Galactic curves for HD 62542, HD 73882, and HD 210121 (Paper I); nevertheless, those curves match the FM fits within the formal uncertainties [approximately 14% in  $A(\lambda)/A(V)$  across the *FUSE* band] and we feel that it would not be appropriate to speculate further about the origin of these features until a larger data sample is compiled.

The FUV extinction curve for Sk -69°228 is very noisy, which would usually indicate a poor match with its unreddened comparison star, but this same star is a good match through the UV. The problem seems to arise with a complex of photospheric Fe III lines evident in the comparison star spectrum, Sk -65°15. An examination of intermediate continuum

segments demonstrates that the reddened and comparison stellar spectra have very similar shapes aside from these lines, and that connecting the lower wavenumber portion of this star’s FUV extinction curve with the two highest wavenumber points would be a reasonable approximation. Notably, this procedure results in an FUV curve that is consistent with an extension of the UV FM fit, despite the impression that a small offset is still present after the *FUSE* flux adjustment. The curve is still included in further analysis for the sake of completeness and because our comparison sample is limited, but we note that the mean curve derived for the LMC2 group, which includes this path, is consistent with the other curves in the group unaffected by any taint of mismatch. On the whole, the ease with which the UV and FUV extinction curves line up for our Magellanic Cloud sight lines complements the results for Milky Way sight lines; namely, that most Galactic sight lines also seem to show FUV extinction that is a good extrapolation of the FM fits made to the extinction curves in the UV. Agreement between the CCM relation and FUV extinction, however, has proved less ubiquitous. For instance, Buss et al. (1994) found that the FUV extinction for two Galactic sight lines with large ( $\rho$  Oph) and small (HD 25443) values of  $R_V$  follow CCM closely, but that there are exceptions; one notable example is the bright-nebula sight line toward HD 37903 which shows a steeper extinction in the FUV, based on *Copernicus* data, than would be predicted by CCM. Paper I, which included paths such as HD 210121 and HD 62542 that do not follow CCM in the UV, came to similar conclusions. Although the UV extinction curves for each sight line they studied could be smoothly extrapolated into the FUV using an FM fit, only three paths that followed CCM through UV wavelengths were also in accord across the FUV. The CCM relations for four others from Paper I either over or underestimated their FUV extinction, as small discrepancies in the UV became more pronounced at shorter wavelengths, and the two non-CCM curves diverged more strongly from their  $R_V$ -based curves with increasing wavenumber. Because the LMC and SMC curves do not have a CCM-like wavelength dependence and because the S/N ratios of the individual extinction curves are relatively low, subtle variations in the FUV slope such as those seen by Buss et al. (1994) cannot be ruled out.

### 3.3. FUV MEM Modelling: Grain Properties

To increase the S/N for MEM modelling purposes, we have constructed average extinction curves for the LMC average and LMC2 regions outlined by Misselt et al. 1999 (see Table 6); the curves are plotted in Figure 6. The two sight lines in the SMC, which represent the bar and wing regions, are considered individually. Using the two average LMC curves and the two SMC curves, we have extended the dust-grain population analysis of Clayton et al. (2003) into the FUV. We employ a (slightly) modified version of the MEM

extinction-fitting algorithm (Kim et al. 1994; Kim & Martin 1996). Instead of using the number of grains of a given size to describe the dust population, the algorithm employs the mass distribution in which  $m(a)da$  is the mass of dust grains per H atom in the size interval from  $a$  to  $a+da$ . Thus, the traditional MRN-type model (Mathis, Rumpl, & Nordsieck 1977) becomes  $m(a) \propto a^{-0.5}$ . We use a power law with exponential decay (PED) as the template function for each component. The data are examined at 34 wavelengths, and the grain cross sections are computed over the range 0.0025–2.7  $\mu\text{m}$  with 50 logarithmically spaced bins. The shape of the mass distribution is strongly constrained only for data over the interval 0.02–1  $\mu\text{m}$ . Below 0.02  $\mu\text{m}$ , the Rayleigh scattering behavior constrains only total mass; above 1  $\mu\text{m}$ , the "grey" nature of the dust opacity also forces the MEM algorithm to simply adjust the total mass, using the shape of the template function to specify the size dependence of the distribution. The total mass of dust is constrained using both the gas-to-dust ratio and "cosmic" abundances (i.e., we try not to use more carbon or silicon than is available). The elemental abundance standards used in this analysis are those adopted in Paper I for the Galaxy (358 and 35 atoms per million H for C and Si, respectively), and by Clayton et al. (2003) for the LMC and SMC (110 and 65 for the LMC and 54 and 11 atoms per million H for the SMC); Table 7 reports the values of the gas-to-dust ratios used here for the LMC and SMC. We consider only three-component models of homogeneous, spherical grains: modified "astronomical silicate" (Weingartner & Draine 2001), amorphous carbon (Zubko et al. 1996), and graphite (Laor & Draine 1993). While it must be acknowledged that the three grain component system we have used to model these extinction curves is simpler than might be expected of actual interstellar dust, the results can be quite useful for identifying grain population properties that distinguish sight lines from one another. The same component-specific PED constraints (e.g., the onset of the exponential cutoff) adopted in Paper I were utilized for the current modelling.

The MEM fits to FM parameterizations of the average Magellanic Cloud extinction curves listed in Table 6 are presented in Figures 7 and 8. The first plot shows the amount of extinction provided by the three distinct grain components, as well as the total extinction of the model, compared to the FM fit associated with each extinction curve. The error bars plotted on these fits are indicative of the mean gap between the FM fit and the underlying extinction curve in each wavelength bin. The fractions of the adopted elemental abundances available for each grain component that are required by the best MEM fit are listed in Table 8. Figure 8 depicts the corresponding mass distributions for different sizes of grains belonging to each model component relative to the mass of hydrogen.

The proportions of the available silicon and carbon used in the MEM fits to the various FM parameterizations cover a very wide range, as was seen in fits to IR through UV data alone by Clayton et al. (2003). Three general factors determine the fraction of silicon and

carbon that any individual sight line will use. First, the higher the gas-to-dust ratio is, the more metals are available in the gas phase. Second, the higher the abundances of metals are, the more material is available. Finally, high values of  $R_V$  imply a greater than average mass fraction in larger grains which are not as efficient per unit mass as smaller grains. For instance, it can be seen from the MEM fits that the SMC wing (AzV 456), which has a low gas-to-dust ratio and low elemental abundances relative to the Galaxy, uses more than 100% of the available silicon. However, the LMC2 and the SMC bar (AzV 18) regions, which also have both low elemental abundances but are characterized by higher gas-to-dust ratios, use less than half the amount of available silicon that the LMC Avg and SMC wing regions require and also significantly less carbon.

A recent observation has suggested that silicon is relatively undepleted in the SMC bar (Welty et al. 2001). However, model fits to the average SMC bar extinction indicate that its curve cannot be fitted with carbon grains alone (Weingartner & Draine 2001; Clayton et al. 2003). Figures 7 and 8 clearly show that this conclusion is born out in the current fits. SMC extinction for both bar and wing is very steep in the FUV, necessitating the presence of a large population of small grains. Yet because the 2175 Å bump is absent in the bar region, small ( $a < 0.02\mu\text{m}$ ) carbon grains do not meet the SMC FUV extinction requirements; thus, silicates play a very important role in the models. Even our SMC wing sight line, whose extinction curve follows CCM reasonably well, places a much higher demand on silicon reserves than carbon: a typical Galactic curve conforming to CCM allows graphite to fulfill a significant part in FUV extinction due to the strength of its UV bump, but the SMC wing bump is somewhat weaker than the  $R_V=2.19$  CCM curve would imply. The next steepest sight lines, in the LMC, do not show much difference in demand from a typical Galactic curve (HD 14250 was chosen from Paper I for illustration purposes), once the gas-to-dust ratio differences are taken into account. Typically, carbon grains are responsible for most of the visible extinction and silicon grains for most of the UV extinction; therefore, in general, both species of grains are needed along any sight line to get a good fit to the extinction curve. Apart from deficits of large silicate and carbon grains in the SMC, the MEM analysis of the Magellanic Cloud FUV extinction produces results similar to those derived from an analysis of several Galactic sight lines (Paper I). The Galactic sight lines, like the SMC wing or LMC Avg, are more likely to use more than 100% of the available silicon and/or carbon. Among these sight lines, the strength of the 2175 Å bump in relation to the FUV rise is the factor that distinguishes whether the stiffer abundance demand is placed on silicon or carbon. Likewise, the element most demanded by the SMC bar sight line and the mean LMC2 curve is determined by this factor, although the minimal presence of the bump in these curves allows the modelling to make more efficient use (especially in small grains) of the available elements.

The general structure in the size vs  $m(a)$  curves for extinction out to  $8 \mu\text{m}^{-1}$  for the Magellanic Cloud sight lines does not change much when the *FUSE* data are included. Figures 7 and 8 showing the MEM fits and size vs  $m(a)$  curves cannot be directly compared to Figure 3 of Clayton et al. (2003) because there are differences in the input parameters such as the gas-to-dust ratios. But the MEM models run with the same input parameters for extinction curve that are cutoff at  $8 \mu\text{m}^{-1}$  and those shown here, which extend to  $10 \mu\text{m}^{-1}$ , are quite similar; there is at most a few percent difference in the amount of silicon and carbon required by the two sets of models for the four SMC and LMC curves. The structure evident in the mass distributions of Figure 8 particularly identify grain sizes for which each component in our simple model can account for the detailed shape of each extinction curve. For instance, the two peaks in the amorphous carbon distribution for HD 14250 correspond roughly to maxima appearing in the silicate distribution of Kim et al. (1994) in their silicate-graphite model. These authors ascribe the peaks to the requirements of fitting the optical and UV portions of the extinction curve using the spectral wavelength dependence appropriate to each of the two grain components in their model. In the case of AzV 456 (the SMC wing), however, efforts to reproduce the extinction curve using this three-component model appear to require dramatic peaks and dips in the mass distribution as a function of grain size. Aside from this curve, however, the scale of structure in the distribution is consistent with levels noted by previous studies (Kim et al. 1994; Clayton et al. 2003). For AzV 456, the solution requires that the graphite distribution be strongly peaked in order to account for the  $2175 \text{ \AA}$  bump and provide as much extinction as possible at FUV wavelengths. Since the FUV portion of this curve extends, or even amplifies, the steep rise at the short-wavelength end of the previous IR through UV result (Clayton et al. 2003), there is no relaxation of the demand on silicon reserves. Specifically, when comparing MEM solutions for the SMC wing curve with and without the *FUSE* data, nearly identical proportions of the available silicon and carbon are utilized. The only notable distinction between the two solutions is that a few percent of the amorphous carbon demand is shifted to graphite when the FUV data are included. The extinction curves for our other groups also smoothly extend from the UV into FUV wavelengths, and the models derived from IR-to-UV and IR-to-FUV data require almost precisely the same amounts of silicon and carbon be present in dust grains. The similarity in the MEM results for these two sets of models may be due to the efficiency of the small grains in FUV extinction, in that large numbers of such grains are not needed, or perhaps the observed amounts of FUV extinction can be provided by the larger grains which are also important for extinction at longer wavelengths. This issue will be investigated further as we study the distinction between global and sight-line-specific FUV extinction characteristics of using a much larger number of sight lines, in a future paper.



#### 4. Conclusion

This paper is the second in a series investigating the FUV characteristics of extinction due to interstellar dust. The first paper dealt with a small sample of Galactic sight lines with a variety of  $R_V$  values, including paths whose extinction does not conform to the CCM parameterization. This paper examined a similarly-sized set of sight lines probing the Small and Large Magellanic Clouds, with the goal of determining how the addition of FUV data to their corresponding extinction curves affected models of Magellanic Cloud dust grain properties.

Using *FUSE* observations of four stars in the SMC and 12 stars in the LMC, we were able to construct two extinction curves for the SMC and seven representing the LMC. Despite the poor quality of the data for some of the reddened stars, molecular hydrogen was measured for each sight line and their corresponding absorption features were removed from consideration in the extinction analysis. Flux mismatches between *IUE* and *FUSE* data, likely due to poor S/N values in the affected observations, were alleviated by rescaling the entire *FUSE* spectrum. Comparison of the resulting FUV extinction with the curve constructed only through wavelengths observed by *IUE* demonstrated that the FUV portions were generally consistent with a smooth extrapolation of the IR-to-UV curve. Nevertheless, we note that a “kink” appeared in the AzV 456 curve, similar to much smaller features present in curves analysed in Paper I. We plan to address the existence and nature of this kink in a subsequent paper examining the variation in properties of FUV extinction.

It was anticipated that including FUV data in the MEM analysis of the Magellanic Cloud dust grain population might give rise to significantly different properties than Galactic dust since the FUV rise in the Clouds is generally much steeper than it is in the Milky Way, and the UV bump is smaller. However, aside from some complex structure likely driven by the simplicity of our grain component model, the sight lines through the Clouds exhibiting Galactic-like extinction are similar to Galactic paths in that they demand 100% or more of the available carbon and/or silicon. The only real differences between the populations for these galaxies are that the SMC wing sight line has a much smaller grain size cutoff for astronomical silicates and amorphous carbon and a generally smaller dust mass. MEM solutions for the sight lines through the Clouds that exhibited more distinctly Magellanic-Cloud-type extinction were able to satisfy their curves using smaller proportions of the elements available to them; the SMC bar solution, like that for the SMC wing, is characterized by a smaller grain size cutoff and lower dust mass than Galactic or LMC solutions. The addition of the *FUSE* data to the analysis does not dramatically alter the properties of each dust population, except to shift small amounts of the carbon demand between amorphous carbon and graphite.

The molecular hydrogen abundances determined in the process of constructing the full IR-to-FUV extinction curves supplement those already appearing in the literature. Although the emphasis has been on eliminating H<sub>2</sub> absorption features from the spectra rather than deriving robust column density measurements, our results are consistent with the larger recent survey of molecular hydrogen in the Magellanic Clouds by Tumlinson et al. (2002) and we complement their paths by probing several sight lines with larger column densities. Among these sight lines,  $E(B-V)/N(\text{H I})$  ratios are generally reduced relative to Galactic values while  $E(B-V)/N(\text{H}_2)$  are roughly the same, implying somewhat lower  $f(\text{H}_2)$ -values in the Clouds than are typical in the Milky Way for similar degrees of reddening.

This study was supported by NASA grant NAG5-108185.

## REFERENCES

- Black, J. H., & Dalgarno, A. 1976, ApJ, 203, 132
- Bouchet, P., Lequeux, J., Maurice, E., Prévot, L., & Prévot-Burnichon, M. L. 1985, A&A, 149, 330
- Browning, M. K., Tumlinson, J., & Shull, J. M. 2003, ApJ, 582, 810
- Buss, R. H., Jr., Allen, M., McCandliss, S., Kruk, J., Liu, J., & Brown, T. 1994, ApJ, 430, 630
- Cardelli, J. A., Clayton, G. C., & Mathis, J. S. 1989, ApJ, 345, 245 (CCM)
- Clayton, G. C., Green, J., Wolff, M. J., Zellner, N. E. B., Code, A. D., Davidsen, A. F., WUPPE Science Team, & HUT Science Team 1996, ApJ, 460, 313
- Clayton, G. C., Wolff, M. J., Sofia, U. J., Gordon, K. D., & Misselt, K. A. 2003, ApJ, 588, 871
- Diplas, A., & Savage, B. D. 1994, ApJ, 427, 274
- Draine, B. T. 2003, ARA&A, 41, 241
- Fitzpatrick, E. L. 1985a, ApJ, 299, 219
- Fitzpatrick, E. L. 1985b, ApJS, 59, 77
- Fitzpatrick, E. L. 1986, AJ, 92, 1068

- Fitzpatrick, E. L., & Massa, D. M. 1990, *ApJS*, 72, 163
- Gordon, K. D., & Clayton, G. C. 1998, *ApJ*, 500, 816
- Gordon, K. D., Clayton, G. C., Misselt, K. A., Landolt, A. U., & Wolff, M. J. 2003, *ApJ*, 594, 279 (G03)
- Green, J. C., Snow, T. P., Jr., Cook, T. A., Cash, W. C., & Poplawski, O. 1992, *ApJ*, 395, 289
- Gunderson, K.S., Clayton, G.C., & Green, J.C. 1998, *PASP*, 110, 60
- Hutchings, J. B., & Giasson, J. 2001, *PASP*, 113, 1205
- Jenkins, E. B., Savage, B. D., & Spitzer, L. 1986, *ApJ*, 301, 355
- Jura, M. 1974, *ApJ*, 191, 375
- Jura, M. 1975, *ApJ*, 197, 581
- Kim, S.-H., Martin, P. G., & Hendry, P. D. 1994, *ApJ*, 422, 164
- Kim, S.-H., & Martin, P. G. 1996, *ApJ*, 462, 296
- Koornneef, J., & Code, A. D. 1981, *ApJ*, 247, 860
- Koornneef, J. 1982, *A&A*, 107, 247
- Laor, A., & Draine, B. T. 1993, *ApJ*, 402, 441
- Lewis, N. K., Cook, T. A., & Chakrabarti, S. 2005, *ApJ*, 619, 367
- Longo, R., Stalio, R., Polidan, R. S., & Rossi, L. 1989, *ApJ*, 566, 267
- Massa, D., & Fitzpatrick, E. L. 2000, *ApJS*, 126, 517
- Massa, D., Savage, B.D., & Fitzpatrick, E. L. 1983, *ApJ*, 266, 662
- Massey, P. 2002, *ApJS*, 141, 81
- Misselt, K. A., Clayton, G. C., & Gordon, K. D. 1999, *ApJ*, 515, 128
- Mathis, J. S., Rumpl, W., & Nordsieck, K. H. 1977, *ApJ*, 217, 425
- Nandy, K., Morgan, D. H., Willis, A. J., Wilson, R., Gondhalekar, P. M., & Houziaux, L. 1980, *Nature*, 283, 725

- Oestreicher, M. O., Gochermann, J., & Schmidt-Kaler, T. 1995, *A&AS*, 112, 495
- Rachford, B. L., Snow, T. P., Tumlinson, J., Shull, J. M., Roueff, E., André, M., Désert, J.-M., Ferlet, R., Vidal-Madjar, A., & York, D. G. 2001, *ApJ*, 555, 839
- Rachford, B. L., Snow, T. P., Tumlinson, J., Shull, J. M., Blair, W. P., Ferlet, R., Friedman, S. D., Gry, C., Jenkins, E. B., Morton, D. C., Savage, B. D., Sonnentrucker, P., Vidal-Madjar, A., Welty, D. E., & York, D. G. 2002, *ApJ*, 577, 221
- Rocca-Volmerange, B., Prévot, L., Prévot-Burnichon, M. L., Ferlet, R., Lequeux, J. 1981, *A&A*, 99, L5
- Sahnow, D. J., Moos, H. W., Ake, T. B., Andersen, J., Andersson, B.-G., André, M., Artis, D., Berman, A. F., Blair, W. P., Brownsberger, K. R., Calvani, H. M., Chayer, P., Conard, S. J., Feldman, P. D., Friedman, S. D., Fullerton, A. W., Gaines, G. A., Gawne, W. C., Green, J. C., Gummin, M. A., Jennings, T. B., Joyce, J. B., Kaiser, M. E., Kruk, J. W., Lindler, D. J., Massa, D., Murphy, E. M., Oegerle, W. R., Ohl, R. G., Roberts, B. A., Romelfanger, M. L., Roth, K. C., Sankrit, R., Sembach, K. R., Shelton, R. L., Siegmund, O. H. W., Silva, C. J., Sonneborn, G., Vaclavik, S. R., Weaver, H. A., Wilkinson, E. 2000a, *ApJ*, 538, L7
- Sahnow, D. J., Gummin, M. A., Gaines, G. A., Fullerton, A. W., Kaiser, M. E., & Siegmund, O. H. 2000b, *Proc. SPIE*, 4139, 149
- Sasseen, T. P., Hurwitz, M., Dixon, W., V., & Airieau, S. 2002, *ApJ*, 566, 267
- Savage, B. D., Bohlin, R. C., Drake, J. F., & Budich, W. 1977, *ApJ*, 216, 291
- Savage, B. D., & Mathis, J. S. 1979, *ARA&A*, 17, 73
- Schwering, P. B. W., & Israel, F. P. 1991, *A&A*, 246, 231
- Shull, J. M., Tumlinson, J., Jenkins, E. B., Moos, H. W., Rachford, B. L., Savage, B. D., Sembach, K. R., Snow, T. P., Sonneborn, G., York, D. G., Blair, W. P., Green, J. C., Friedman, S. D., & Sahnow, D. J. 2000, *ApJ*, 538, L73
- Snow, T. P., Jr., Allen, M. M., Polidan, R. S. 1990, *ApJ*, 359, L23
- Snow, T. P., Jr., & York, D. G. 1975, *Ap&SS*, 34, 19
- Sofia, U. J., Wolff, M. J., Rachford, B. L., Gordon, K. D., Clayton, G. C., Cartledge, S. I. B., Martin, P. G., Draine, B. T., Mathis, J. S., Snow, T. P., & Whittet, D. C. B. 2005, *ApJ*, *accepted* (Paper I)

- Tumlinson, J., Shull, J. M., Rachford, B. L., Browning, M. K., Snow, T. P., Fullerton, A. W., Jenkins, E. B., Savage, B. D., Crowther, P. A., Moos, H. W., Sembach, K. R., Sonneborn, G., & York, D. G. 2002, *ApJ*, 566, 857
- Weingartner, J. C., & Draine, B. T. 2001, *ApJ*, 548, 296
- Welty, D. E., Hobbs, L. M., & York, D. G. 1991, *ApJS*, 75, 425
- Welty, D. E., Lauroesch, J. T., Blades, C., Hobbs, L. M., & York, D. G. 2001, *ApJ*, 554, L75
- York, D. G., Drake, J. F., Jenkins, E. B., Morton, D. C., Rogerson, J. B., & Spitzer, L. 1973, *ApJ*, 182, L1
- Zubko, V. G., Menella, V., Colangeli, L., & Bussoletti, E. 1996, *MNRAS*, 282, 1321

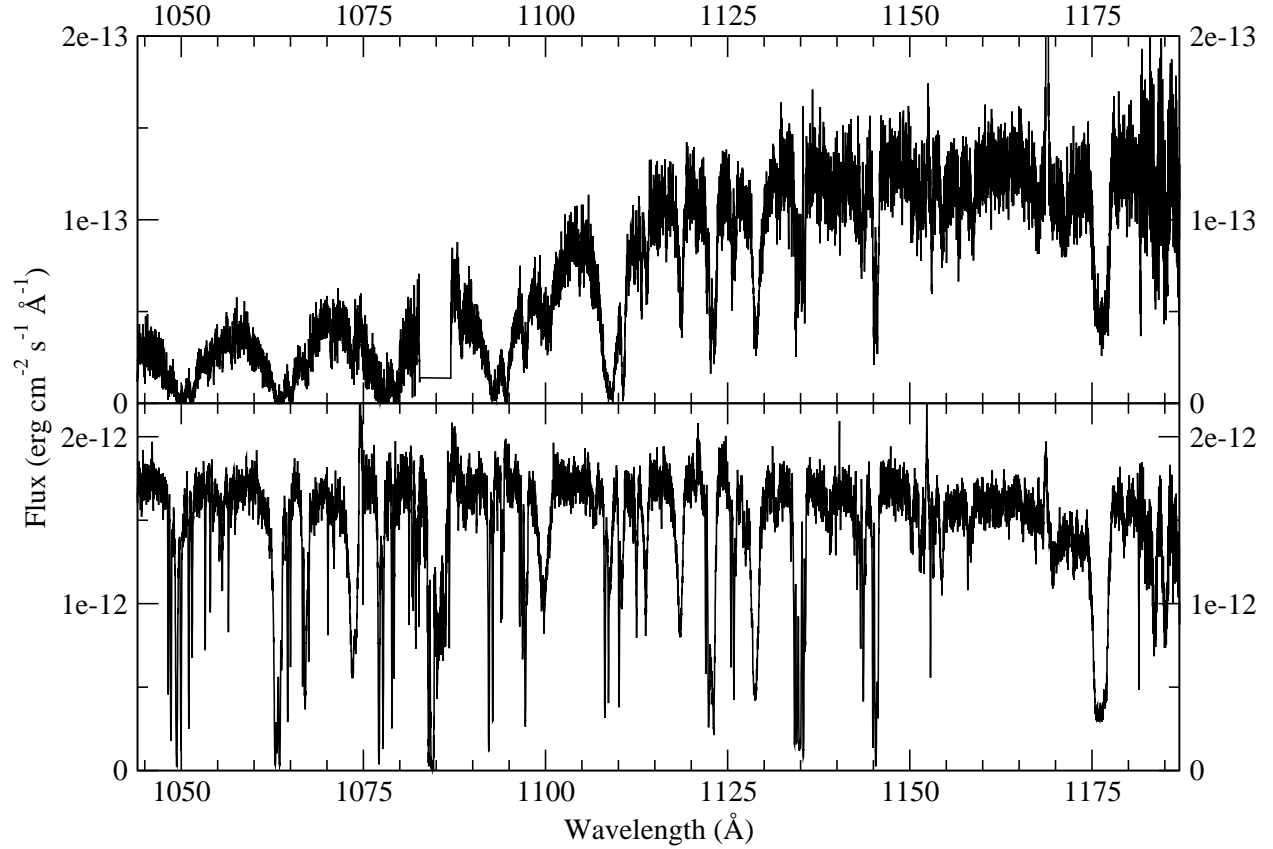


Fig. 1.— Sample *FUSE* spectra.

Sample *FUSE* spectra are plotted above, including an example of poor quality data in the upper panel (for AzV 456) and fine quality data in the lower panel (for AzV 70); these spectra also comprise an extinction pair. Of further note, the AzV 456 continuum drops dramatically between 1080 and 1120 Å, giving rise to a peculiar kink in the extinction curve discussed later in the text.

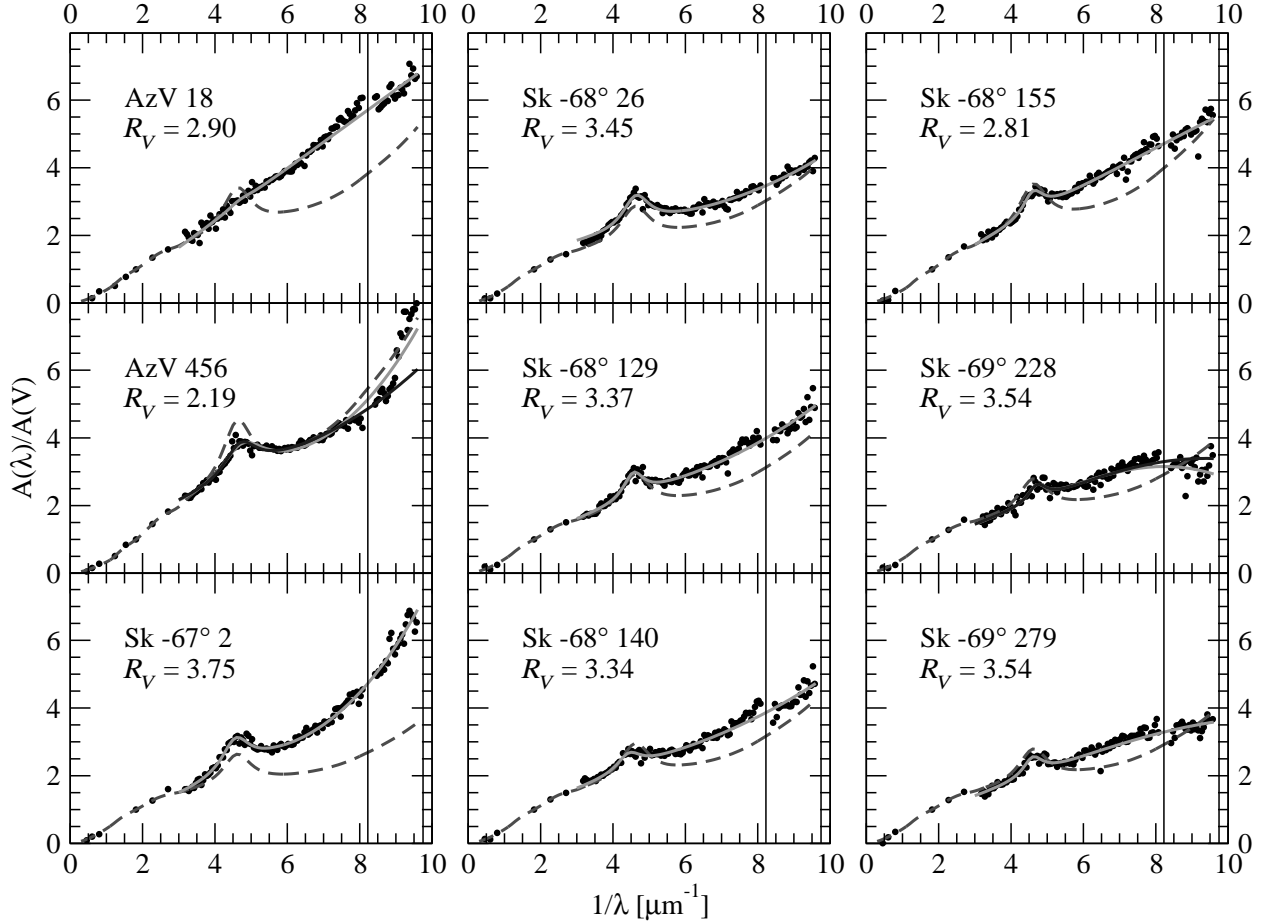


Fig. 2.— Magellanic Cloud Extinction Curves.

The extinction curves for each of the reddened/unreddened star pairs in Table 1 are plotted above; IR, optical, UV (from *IUE*), and FUV (from *FUSE*) data are all included. A CCM curve based on the  $R_V$  value derived from the IR and optical portions of each extinction curve is also plotted using a dashed line, and the FM fit to the full curves are indicated in each panel by solid grey lines. In each case but AzV 456 and Sk -69°228, the FM fit for only IR through UV data almost precisely overlaps the FM fit to the full curve. For these two exceptions, the IR-to-UV fit is represented by a solid dark line. The vertical lines identify central wavelengths for Ly $\alpha$  and Ly $\beta$ .

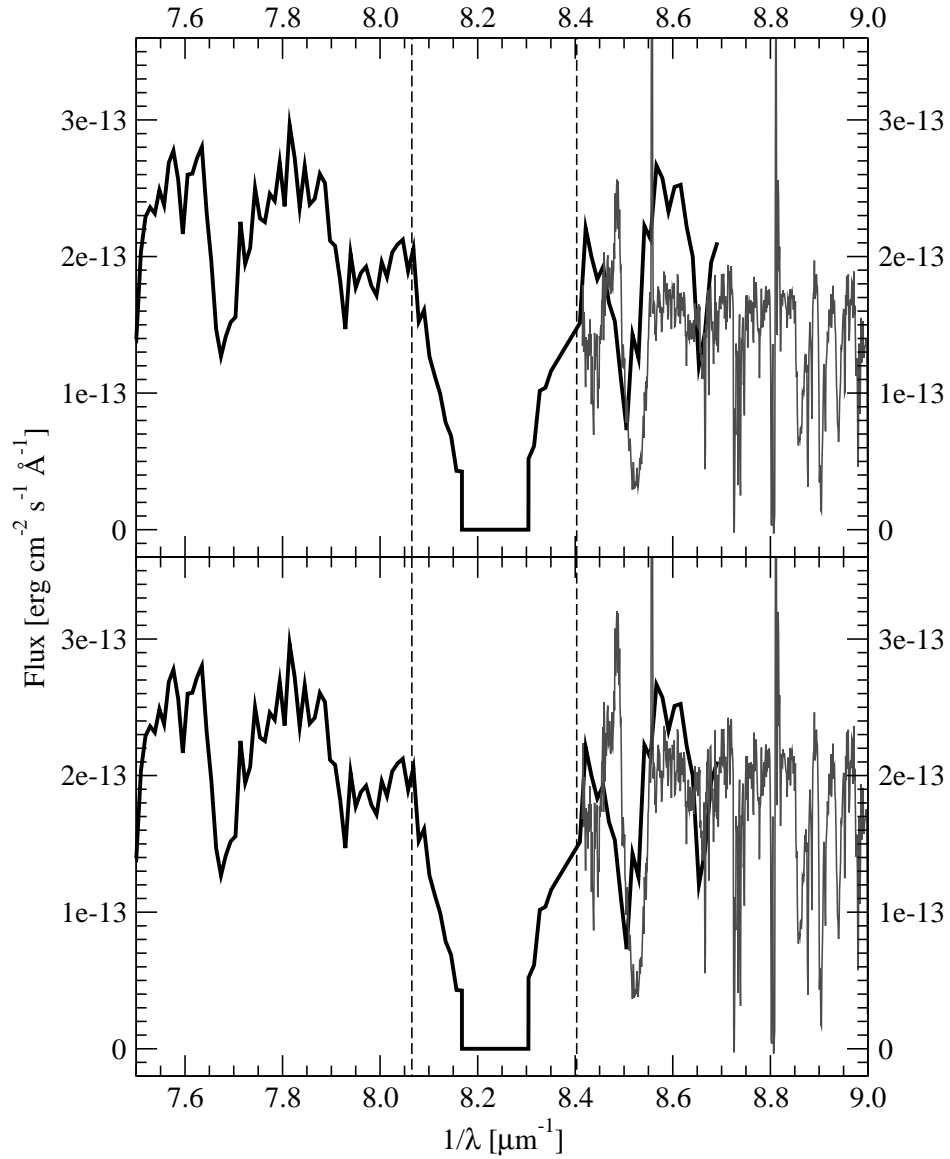


Fig. 3.— Sk -69°228 Spectral Match.

*IUE* and *FUSE* spectra in a region that includes these instruments' overlapping wavelength coverage have been plotted above for the star Sk -69°228; *IUE* fluxes are represented by the heavy solid line and the light grey line signifies *FUSE* data. The top and bottom panels depict the flux levels before and after the linear corrections were applied. These corrections generally reduced the size of extinction curve offsets between UV and FUV data. The vertical dashed lines delimit portions of the spectrum contaminated by Ly $\alpha$  absorption that have been eliminated from the curves plotted in Figure 2; the central portions have also been set to zero in this plot.



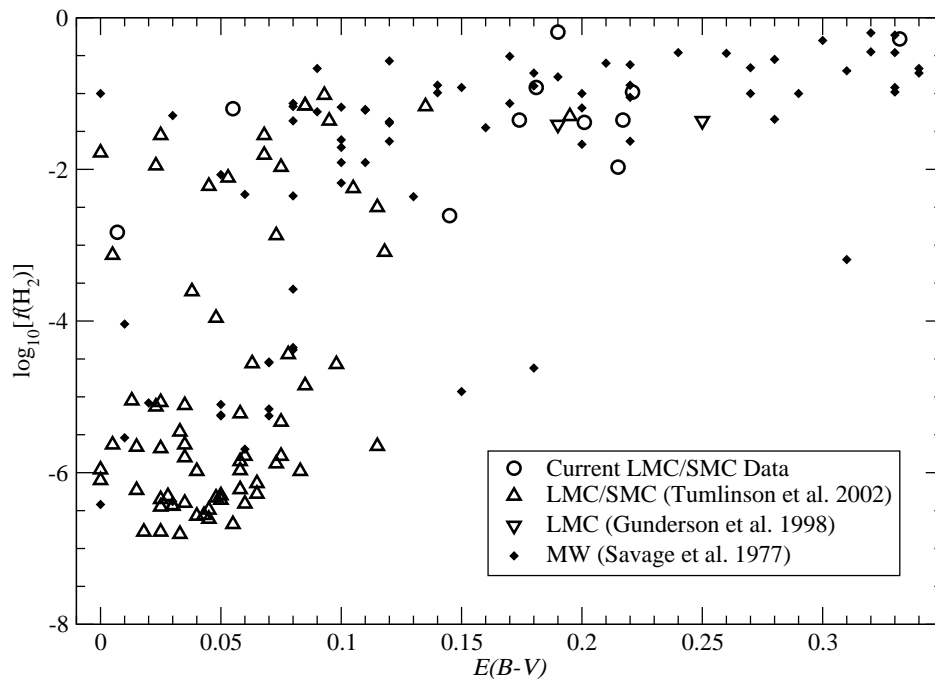


Fig. 4.— Galactic and Magellanic Cloud Molecular Hydrogen Fractions.

The variation of molecular hydrogen fraction  $f(\text{H}_2)$  with color excess  $E(B-V)$  is plotted above for sight lines passing through material associated with the Magellanic Clouds and the Milky Way. The current sample includes stars that are more heavily reddened than the Tumlinson et al. (2002) sample and that emphasize the similarities between how  $f(\text{H}_2)$  relates to  $E(B-V)$  in these galaxies. The label  $E(B-V)$  used in this caption and for the  $x$ -axis in the plot refer to unadjusted values in the Galaxy but  $E'(B-V)$  for Magellanic Cloud sight lines.

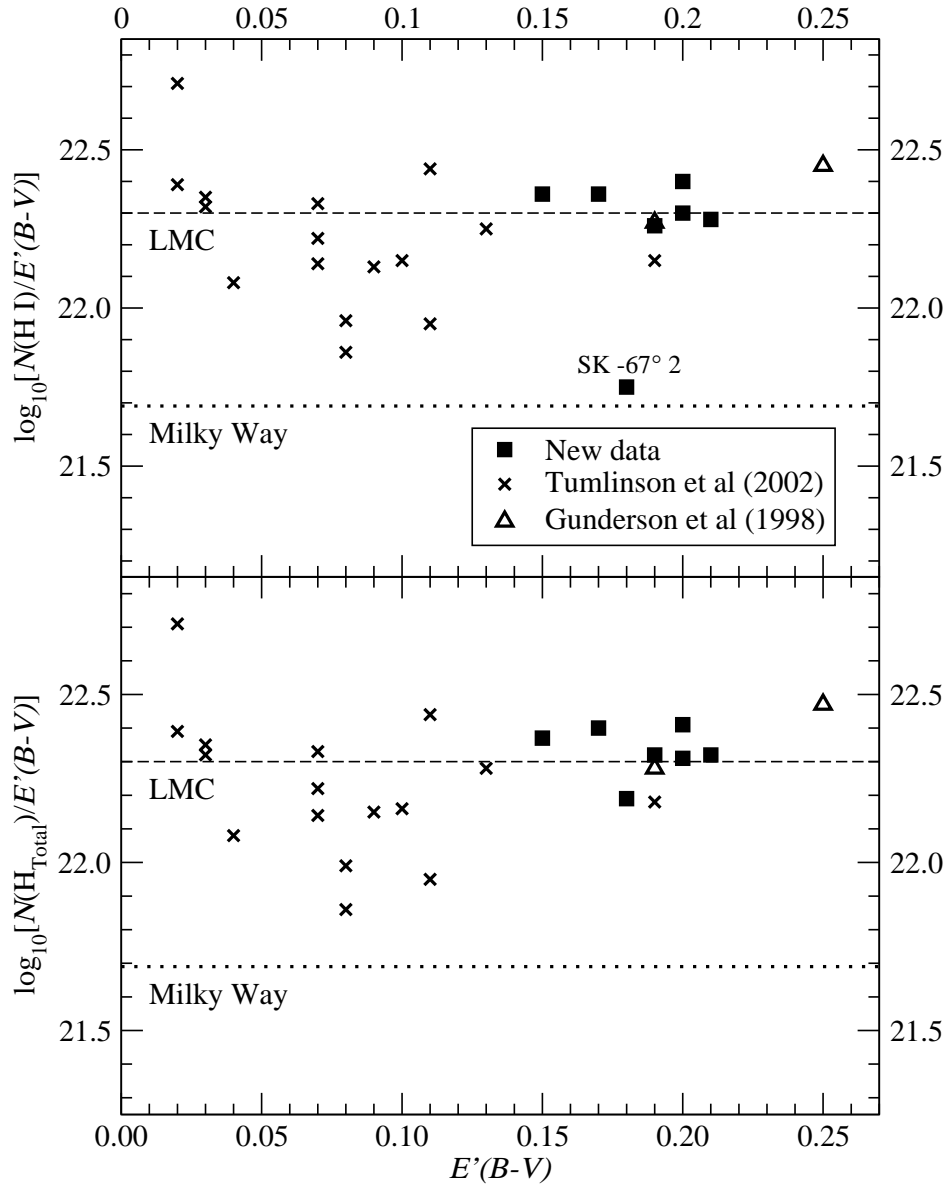


Fig. 5.— LMC Gas-to-Dust Ratios.

Gas-to-dust ratios for LMC extinction pairs are plotted above as a function of  $E(B - V)$ . Of particular note, Sk -67°2 alone among the reddened LMC stars is characterized by a  $\log_{10}[N(\text{H I})/E'(B - V)]$  ratio consistent with that of a Galactic star (dotted line; Diplas & Savage 1994), whereas the corresponding value of  $\log_{10}[N(\text{H}_{\text{Total}})/E'(B - V)]$  agrees with other LMC ratios. The LMC value for  $\log_{10}[N(\text{H I})/E'(B - V)]$  (dashed line; Koornneef 1982) is also plotted in both graphs for reference.

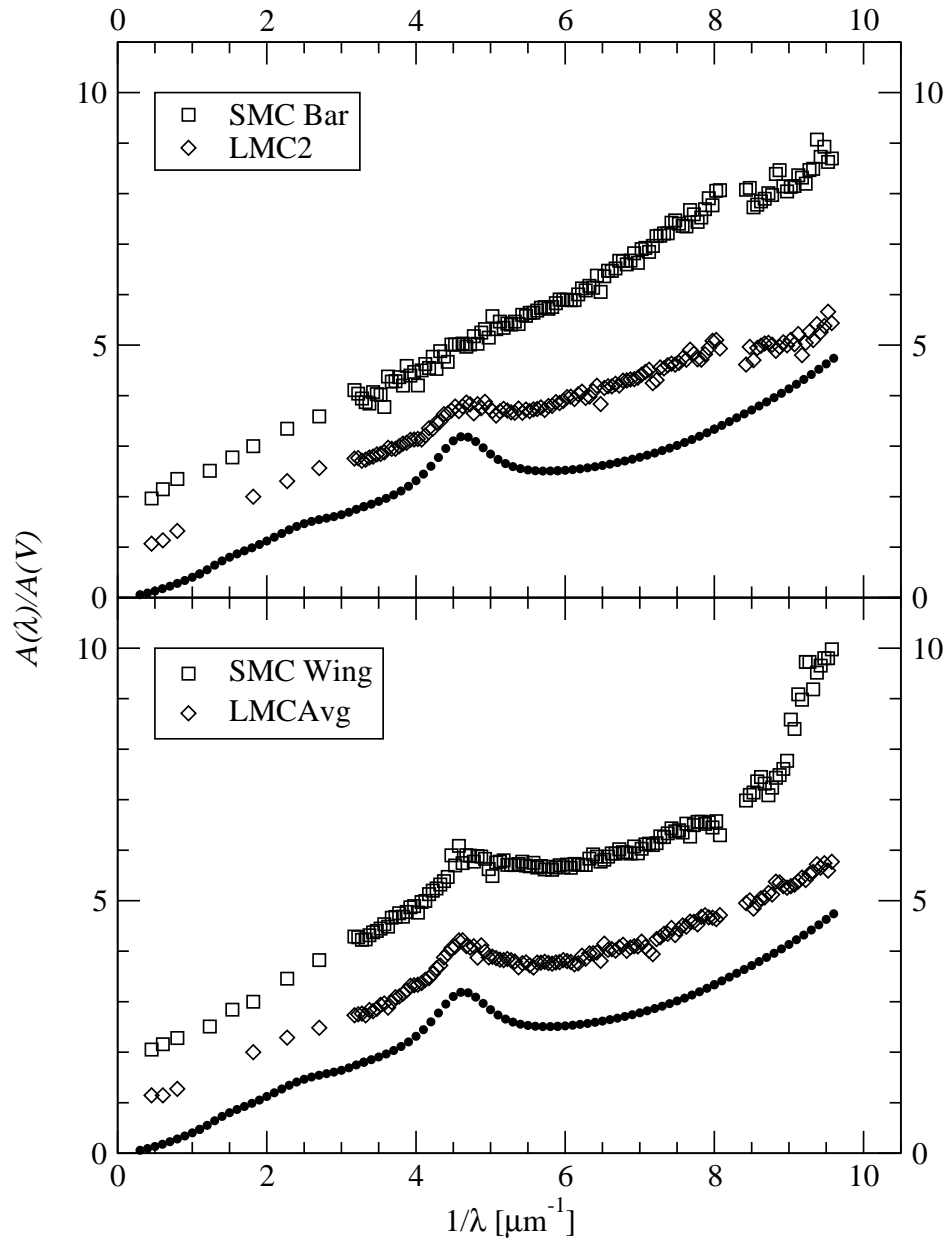


Fig. 6.— Comparing the LMC, SMC, and Galactic Average Extinction Curves. Average extinction curves for the Magellanic Cloud regions LMC2 and SMC bar, those more distinct in character from Galactic extinction, are shown in the upper panel of the above plot; the lower panel depicts the mean curves for the LMC Avg and SMC wing groupings. Both panels include the CCM  $R_V=3.1$  curve in the role of a Galactic reference. The LMC and SMC curves are offset 1 and 2 units in  $A(\lambda)/A(V)$ , respectively, from the Galactic curve in each panel.

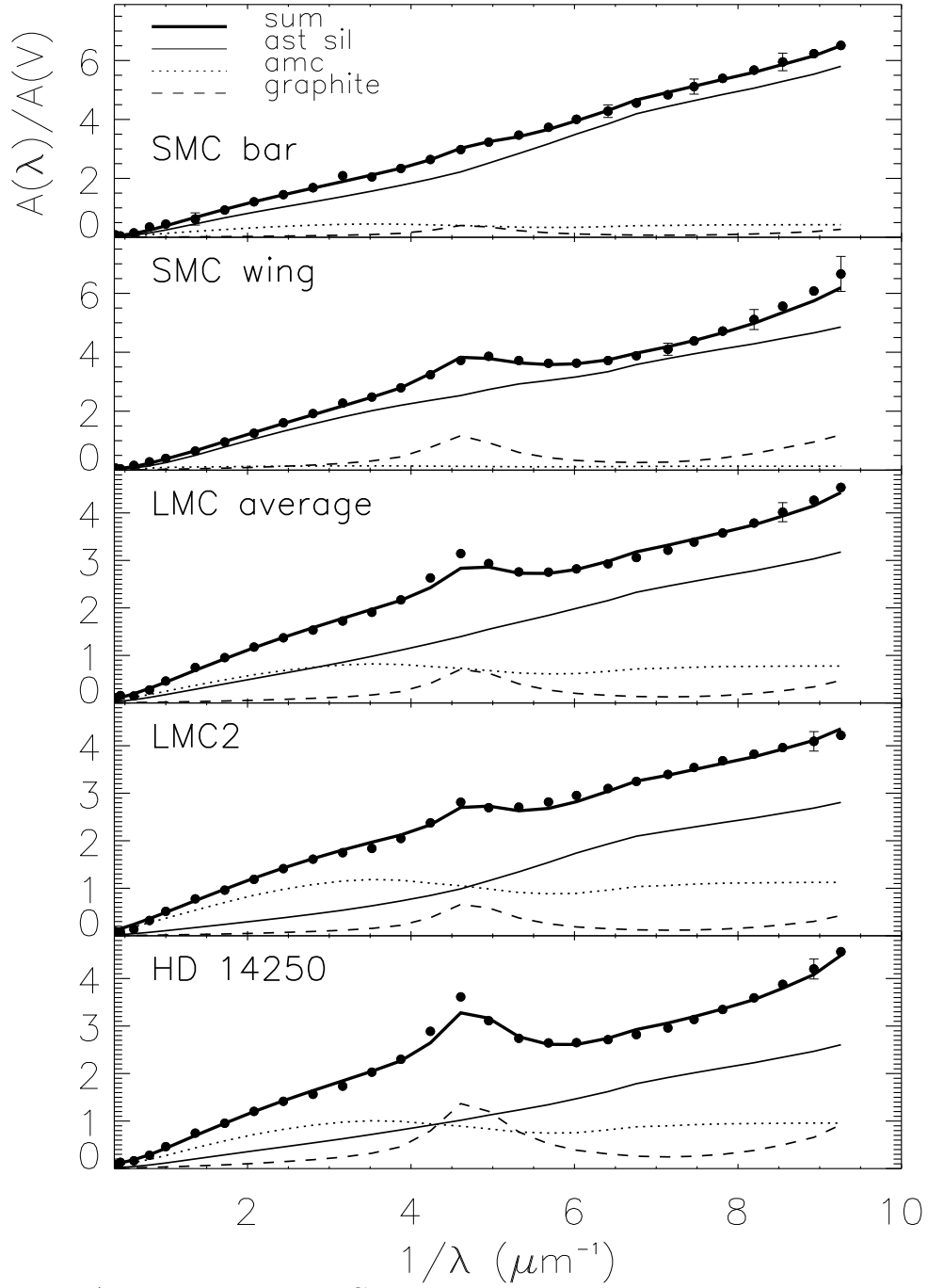


Fig. 7.— MEM Average Extinction Curve Fits.

The MEM fits of astrophysical silicate, amorphous carbon, and graphite dust components to FM parameterizations of the average extinction curves in Figure 6 are plotted above. It should be noted that the MEM models were adjusted to reproduce the FM fit to each extinction curve; consequently, the SMC wing curve does not match the AzV 456/AzV 70 extinction plot of Figure 2 in full detail. The error bars are indicative of the deviation between the FM fit and the extinction curve in nearby bins. For comparison, a typical Galactic sight line is represented in this plot by HD 14250 ( $R_V=2.98\pm 0.14$ ; Paper I).

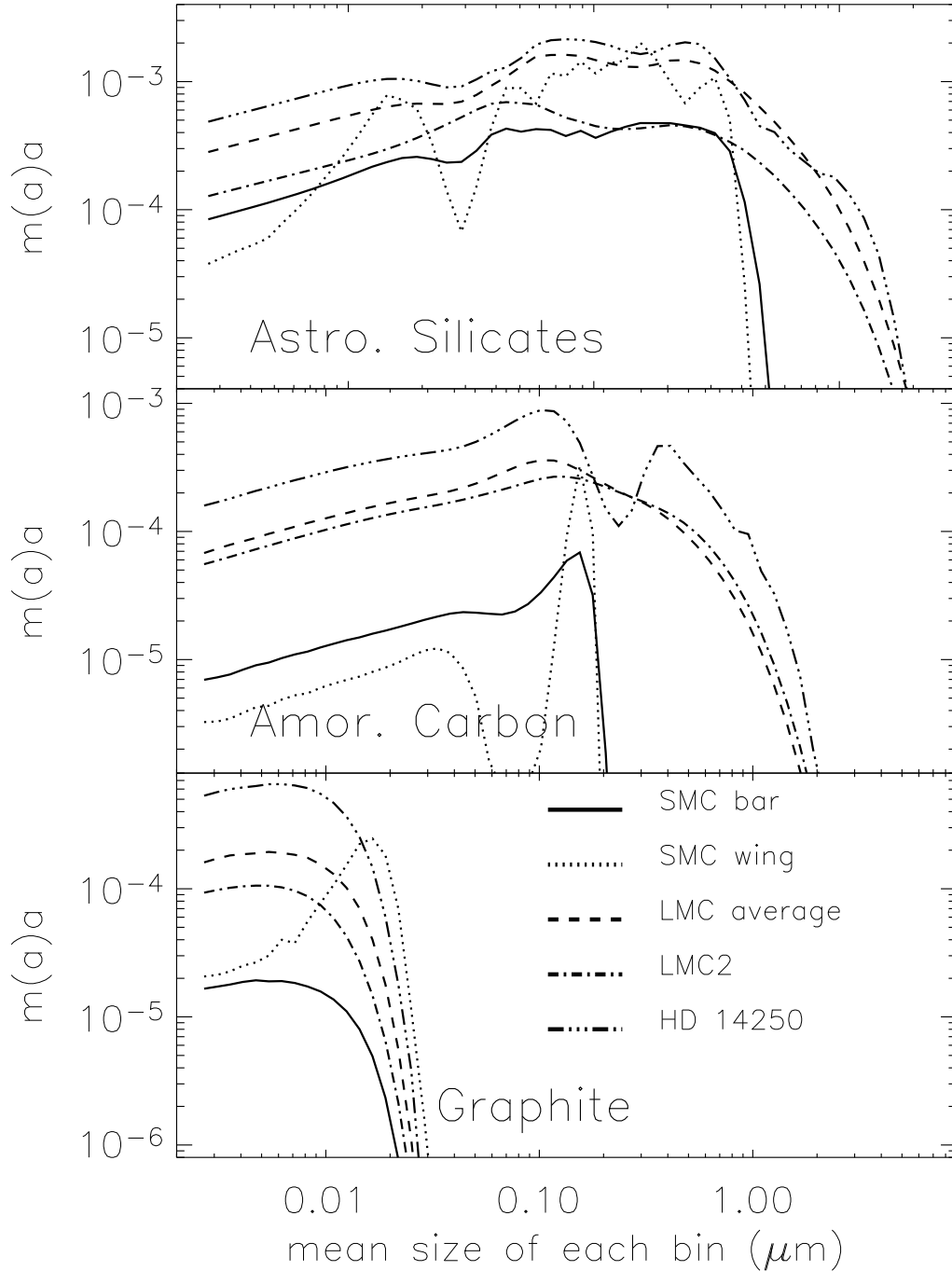


Fig. 8.— MEM Dust Grain Mass Distributions.

The MEM grain size vs  $m(a)da$  functions for each of the average extinction curves of Figure 6 are plotted above. Of particular note, the SMC grain distributions do not include silicate or amorphous carbon grains as large as are required to fit extinction curves in the LMC or the Galaxy. Also, the graphite grain distribution for the SMC wing is strongly peaked by the constraints implied in the bump strength and FUV rise of its extinction curve. As in Figure 7, HD 14250 stands in for a typical Galactic sight line.

Table 1. Extinction Curve Pairs

Reddened Star	Comparison Star	Spectral Type	$\Delta(B-V)$ (mag)	$R_V$	$A_V$ (mag)	$N(\text{H I})/A_V$ ( $10^{21}$ H I atoms/ $A_V$ )
AzV 18	AzV 462	B2 Ia	$0.17\pm 0.03$	$2.90\pm 0.42$	$0.49\pm 0.11$	$17.27\pm 4.30$
AzV 456	AzV 70	O9.7 Ib	$0.26\pm 0.03$	$2.19\pm 0.23$	$0.57\pm 0.08$	$7.01\pm 1.22$
Sk -67°2	Sk -66°35	B2 Ia	$0.15\pm 0.05$	$3.75\pm 0.36$	$0.56\pm 0.23$	$1.78\pm 0.67$
Sk -68°26	Sk -66°35	B3 Ia	$0.19\pm 0.03$	$3.45\pm 0.27$	$0.64\pm 0.16$	$5.46\pm 1.08$
Sk -68°129	Sk -68°41	O9 Ia	$0.17\pm 0.05$	$3.37\pm 0.29$	$0.57\pm 0.22$	$6.98\pm 2.36$
Sk -68°140	Sk -68°41	B0 Ia	$0.20\pm 0.05$	$3.34\pm 0.25$	$0.67\pm 0.22$	$5.99\pm 1.75$
Sk -68°155	Sk -67°168	O8 Ia	$0.20\pm 0.05$	$2.81\pm 0.22$	$0.56\pm 0.18$	$8.88\pm 9.21$
Sk -69°228	Sk -65°15	B2 Ia	$0.15\pm 0.05$	$3.54\pm 0.34$	$0.53\pm 0.23$	$6.60\pm 2.50$
Sk -69°279	Sk -65°63	O9 Ia	$0.21\pm 0.05$	$3.54\pm 0.25$	$0.75\pm 0.23$	$5.38\pm 1.50$

Note. — The Galactic foreground extinction is considered to be comparable for the stars in each pair; consequently, the properties listed in this table are appropriate only to the Magellanic Cloud dust component (Misselt, Clayton, & Gordon 1999). Spectral types refer to the UV classification of each star; the sources are Gordon & Clayton (1998) and Misselt, Clayton, & Gordon (1999).

Table 2. *FUSE* LMC and SMC Observations

Sight Line	<i>FUSE</i> Data Set	Date	Exposure Time (s)
AzV 18	A1180101000	2000 May 29	9293
	B0890101000	2001 Jun 13	45245
AzV 70	A1180202000	2000 Oct 03	2831
	A1180203000	2000 Oct 05	1971
	B0900601000	2001 Jun 15	6152
AzV 456	Q1070101000	2000 Oct 04	3691
	Q1070104000	2000 Oct 06	4903
	Q1070106000	2000 Oct 09	5641
	Q1070102000	2000 Oct 10	2687
	Q1070103000	2000 Oct 12	4352
	P2210201000	2001 Jun 14	8278
AzV 462	A1180301000	2000 Jul 03	5550
Sk -65°15	B0861001000	2001 Nov 17	4293
Sk -65°63	A0490701000	1999 Dec 16	5927
	M1142001000	2000 Sep 26	5581
	B0861101000	2001 Sep 22	4125
Sk -66°35	B1280101000	2001 Oct 25	4030
	B0860301000	2002 Sep 22	4480
Sk -67°2	B0860101000	2001 Aug 14	6935
Sk -67°168	B0860901000	2001 Sep 22	4102
Sk -68°26	B0860201000	2001 Sep 17	11391
Sk -68°129	B0860501000	2001 Sep 22	6681
Sk -68°140	B0860601000	2001 Sep 17	10712
Sk -68°155	B0860701000	2001 Sep 22	8020
Sk -69°228	B0860401000	2001 Sep 23	9422
Sk -69°279	B0860801000	2001 Sep 22	5991





Table 3. Molecular Hydrogen Models: Milky Way

MC Star	$\log_{10} N(\text{H}_2)_{MW}$ ( $\text{cm}^{-2}$ )	$\log_{10} N(0)$ ( $\text{cm}^{-2}$ )	$\log_{10} N(1)$ ( $\text{cm}^{-2}$ )	$\log_{10} N(2)$ ( $\text{cm}^{-2}$ )	$\log_{10} N(3)$ ( $\text{cm}^{-2}$ )	$\log_{10} N(4)$ ( $\text{cm}^{-2}$ )	$\log_{10} N(5)$ ( $\text{cm}^{-2}$ )	$b$ $\text{km s}^{-1}$	$T_{01}^a$ (K)	$T_{ex}^b$ (K)
SMC										
AzV 18	16.57(0.64)	16.33	16.17	14.82	14.27			$8.1^{+2.9}_{-1.9}$	$66 \pm 192$	$187 \pm 296$
AzV 70	18.55(0.05)	18.42	17.95	15.90	15.46	14.66		$4.2^{+0.9}_{-1.6}$	$52 \pm 6$	$357 \pm 786$
AzV 462	15.92(0.16)	15.55	15.48	14.88	14.98			$5.9^{+2.3}_{-4.9}$	$72 \pm 34$	$419 \pm 223$
LMC										
Sk $-65^\circ 15$	18.15(0.06)	17.79	17.86	16.75	16.04			$2.4^{+1.2}_{-1.4}$	$84 \pm 6$	$165 \pm 330$
Sk $-65^\circ 63$	18.00(0.07)	17.75	17.54	16.66	16.56			$1.4^{+1.1}_{-0.4}$	$64 \pm 8$	$303 \pm 263$
Sk $-66^\circ 35$	17.78(0.46)	17.24	17.60	16.34	15.74	14.08		$4.8^{+2.6}_{-2.5}$	$125 \pm 310$	$210 \pm 227$
Sk $-67^\circ 2$	16.83(0.36)	16.56	16.19	15.98	15.81			$6.3^{+5.9}_{-5.2}$	$56 \pm 90$	$277 \pm 197$
Sk $-67^\circ 168$	16.38(0.35)	15.60	16.25	15.24	14.74			$3.5^{+1.2}_{-2.2}$	$200 \pm 95$	$200 \pm 95$
Sk $-68^\circ 26$	16.02(0.35)	15.61	15.32	15.58	14.67			$5.4^{+6.0}_{-4.4}$	$60 \pm 62$	$354 \pm 519$
Sk $-68^\circ 41$	15.31(0.27)	14.31	15.14	14.39	14.31			$4.3^{+4.0}_{-3.3}$	$326 \pm 230$	$326 \pm 230$
Sk $-68^\circ 129$	16.73(0.59)	15.76	16.39	16.15	15.87	15.13		$2.9^{+6.0}_{-1.9}$	$228 \pm 868$	$409 \pm 868$
Sk $-68^\circ 140$	19.01(0.12)	18.54	18.82	17.37	16.28	14.37	14.17	$2.5^{+2.4}_{-1.5}$	$110 \pm 42$	$227 \pm 50$
Sk $-68^\circ 155$	18.35(0.50)	18.26	17.64	15.77	15.36	14.39		$4.6^{+2.2}_{-3.6}$	$47 \pm 133$	$330 \pm 183$
Sk $-69^\circ 228$	18.00(0.20)	17.29	17.80	17.22	16.14			$2.5^{+5.9}_{-1.5}$	$167 \pm 189$	$224 \pm 620$
Sk $-69^\circ 279$	16.17(0.16)	15.70	15.93	14.88	14.71			$8.3^{+5.5}_{-6.0}$	$102 \pm 59$	$277 \pm 308$

<sup>a</sup>The  $\text{H}_2$  kinetic temperature is assumed to be equivalent to  $T_{01}$ , the temperature derived from  $N(J=0)$  and  $N(1)$  assuming a Boltzmann distribution ( $T_{01} = \frac{E_1 - E_0}{k} \frac{\log(\epsilon)}{\log(N(0)/g_0) - \log(N(1)/g_1)}$ ).

<sup>b</sup>The excitation temperature  $T_{ex}$  reflects the sum of effects such as UV photon-pumping and excited state formation, and is identified in this table with the slope of the  $\log[N(J)/g_J]$  vs.  $E(J)$  plot for  $J \geq 2$ .

Note. — This table describes the Milky Way component of the molecular hydrogen models constructed for each target star from the *FUSE* data.

Table 4. Molecular Hydrogen Models: Magellanic Clouds

MC Star	$\log_{10} N(\text{H}_2)_{MC}$ ( $\text{cm}^{-2}$ )	$\log_{10} N(0)$ ( $\text{cm}^{-2}$ )	$\log_{10} N(1)$ ( $\text{cm}^{-2}$ )	$\log_{10} N(2)$ ( $\text{cm}^{-2}$ )	$\log_{10} N(3)$ ( $\text{cm}^{-2}$ )	$\log_{10} N(4)$ ( $\text{cm}^{-2}$ )	$\log_{10} N(5)$ ( $\text{cm}^{-2}$ )	$b$ $\text{km s}^{-1}$	$T_{01}$ (K)	$T_{ex}$ (K)
SMC										
AzV 18	20.36(0.07)	20.13	19.97	17.58	17.79	16.06	15.36	$8.1^{+2.9}_{-1.9}$	$66 \pm 9$	$270 \pm 52$
AzV 456	20.93(0.09)	20.85	20.15	17.67	15.62			$6.0^{+5.9}_{-5.0}$	$45 \pm 4$	$82 \pm 175$
AzV 462	17.65(0.13)	16.65	17.54	16.56	16.16			$2.1^{+1.2}_{-1.1}$	...	$234 \pm 564$
LMC										
Sk $-66^\circ 35$	19.13(0.19)	19.02	18.46	17.02	15.89	14.78	14.26	$4.4^{+3.0}_{-3.1}$	$49 \pm 23$	$302 \pm 152$
Sk $-67^\circ 2$	20.95(0.08)	20.86	20.21	18.41	16.43	15.40		$5.6^{+6.0}_{-4.6}$	$46 \pm 5$	$159 \pm 75$
Sk $-68^\circ 26$	20.38(0.08)	20.20	19.90	18.50	17.76	16.43	15.88	$2.3^{+1.0}_{-1.3}$	$59 \pm 7$	$253 \pm 260$
Sk $-68^\circ 129$	20.05(0.10)	20.00	19.08	18.06	16.65	15.87	15.55	$8.0^{+3.8}_{-4.2}$	$40 \pm 13$	$309 \pm 157$
Sk $-68^\circ 140$	19.50(0.13)	19.09	19.25	18.13	17.45	15.97	15.45	$5.4^{+2.6}_{-2.0}$	$93 \pm 35$	$248 \pm 71$
Sk $-68^\circ 155$	19.99(0.24)	19.75	19.62	17.21	16.37	15.42	14.84	$8.2^{+4.9}_{-3.3}$	$68 \pm 42$	$341 \pm 152$
Sk $-69^\circ 228$	18.70(0.14)	18.28	18.37	17.79	17.13			$3.1^{+6.0}_{-2.1}$	$86 \pm 37$	$249 \pm 555$
Sk $-69^\circ 279$	20.31(0.07)	20.10	19.90	16.46	16.11	15.34		$10.0^{+6.0}_{-6.0}$	$64 \pm 9$	$389 \pm 437$

Note. — This table details the Magellanic Cloud component of the molecular hydrogen models constructed for each target star from the *FUSE* data. The temperatures  $T_{01}$  and  $T_{ex}$  possess the same characteristics as those in Table 3.

Table 5. Flux Shifts

Star	<i>IUE/FUSE</i> Flux Ratio	Star	<i>IUE/FUSE</i> Flux Ratio
AzV 18	1.10	Sk $-67^{\circ}168$	1.05
AzV 70	1.05	Sk $-68^{\circ}26$	0.85
AzV 456	0.85	Sk $-68^{\circ}41$	0.95
AzV 462	1.00	Sk $-68^{\circ}129$	1.00
Sk $-65^{\circ}15$	1.20	Sk $-68^{\circ}140$	1.10
Sk $-65^{\circ}63$	0.85	Sk $-68^{\circ}155$	1.20
Sk $-66^{\circ}35$	1.05	Sk $-69^{\circ}228$	1.25
Sk $-67^{\circ}2$	0.65	Sk $-69^{\circ}279$	1.30

Note. — The table ratios are derived from the calibrated fluxes recorded by each instrument in the spectral overlap from 1150–1185 Å.

Table 6. FM Fit Parameters

Curve	$c_1$	$c_2$	$c_3$	$c_4$	$x_0$	$\gamma$
SMC Bar						
AzV 18	$-4.902 \pm 1.036$	$2.255 \pm 0.436$	$0.165 \pm 0.213$	$0.001 \pm 0.026$	$4.697 \pm 0.078$	$0.738 \pm 0.012$
SMC Wing						
AzV 456	$-0.419 \pm 0.130$	$0.908 \pm 0.094$	$5.026 \pm 1.625$	$0.513 \pm 0.100$	$4.770 \pm 0.079$	$1.470 \pm 0.025$
LMC						
Sk $-66^\circ 19^a$	-4.66	2.02	1.21	0.85	4.54	0.73
Sk $-67^\circ 2$	$-3.479 \pm 1.585$	$1.723 \pm 0.648$	$3.108 \pm 1.296$	$0.881 \pm 0.313$	$4.573 \pm 0.048$	$0.935 \pm 0.016$
Sk $-68^\circ 26$	$0.003 \pm 0.020$	$0.937 \pm 0.150$	$2.581 \pm 0.513$	$0.203 \pm 0.054$	$4.638 \pm 0.049$	$0.898 \pm 0.015$
Sk $-68^\circ 129$	$-2.174 \pm 0.784$	$1.393 \pm 0.443$	$1.184 \pm 0.351$	$0.207 \pm 0.082$	$4.567 \pm 0.071$	$0.688 \pm 0.041$
Average	$-1.704 \pm 0.253$	$1.268 \pm 0.041$	$2.902 \pm 0.187$	$0.266 \pm 0.030$	$4.602 \pm 0.023$	$0.930 \pm 0.015$
LMC2						
Sk $-68^\circ 140$	$-1.929 \pm 0.820$	$1.323 \pm 0.387$	$1.093 \pm 0.525$	$0.161 \pm 0.055$	$4.440 \pm 0.074$	$0.811 \pm 0.014$
Sk $-68^\circ 155$	$-2.842 \pm 0.982$	$1.615 \pm 0.458$	$0.897 \pm 0.336$	$-0.012 \pm 0.013$	$4.611 \pm 0.062$	$0.684 \pm 0.028$
Sk $-69^\circ 228$	$-2.800 \pm 1.219$	$1.449 \pm 0.529$	$0.641 \pm 0.237$	$-0.418 \pm 0.164$	$4.714 \pm 0.079$	$0.609 \pm 0.054$
Sk $-69^\circ 270^a$	-3.51	1.52	0.97	0.24	4.62	0.78
Sk $-69^\circ 279$	$-2.696 \pm 0.857$	$1.364 \pm 0.364$	$0.853 \pm 0.232$	$-0.124 \pm 0.057$	$4.603 \pm 0.077$	$0.664 \pm 0.047$
Average	$-2.487 \pm 0.303$	$1.443 \pm 0.054$	$0.844 \pm 0.140$	$-0.055 \pm 0.016$	$4.586 \pm 0.058$	$0.697 \pm 0.012$

<sup>a</sup>In the interest of providing additional extinction curves for comparison, the data for sight lines previously observed by *Hopkins Ultraviolet Telescope* (Sk  $-66^\circ 19$ ; Sk  $-69^\circ 270$ ; Clayton et al. 1996; Gunderson, Clayton, & Green 1998) have been included in this table.

Table 7. Properties of the Magellanic Cloud ISM

Sight Line or Extinction Pair	$N(\text{H I})$ ( $\text{cm}^{-2}$ )	$N(\text{H}_2)$ ( $\text{cm}^{-2}$ )	$\log_{10} f_{\text{H}_2}$	$E'(B-V)^a$ (mag)	$N(\text{H I})/E'(B-V)$ ( $\text{cm}^{-2} \text{ mag}^{-1}$ )	$N(\text{H}_2)/E'(B-V)$ ( $\text{cm}^{-2} \text{ mag}^{-1}$ )
SMC: individual targets						
AzV 18	$9.0 \times 10^{21}$	$2.3 \times 10^{20}$	-1.35	0.174	$5.2 \times 10^{22}$	$1.3 \times 10^{21}$
AzV 456	$1.5 \times 10^{21}$	$8.5 \times 10^{20}$	-0.28	0.332	$4.5 \times 10^{21}$	$2.6 \times 10^{21}$
AzV 462	$6.0 \times 10^{20}$	$4.5 \times 10^{17}$	-2.83	0.007	$8.6 \times 10^{22}$	$6.4 \times 10^{19}$
SMC: extinction pairs						
AzV 18/AzV 462	$8.5 \times 10^{21}$	$2.3 \times 10^{20}$	-1.29	0.17	$5.0 \times 10^{22}$	$1.4 \times 10^{21}$
AzV 456/AzV 070	$4.0 \times 10^{21}$	$8.5 \times 10^{20}$	-0.53	0.26	$1.5 \times 10^{22}$	$3.3 \times 10^{21}$
LMC: individual targets						
Sk $-66^\circ 35$	$4.0 \times 10^{20}$	$1.3 \times 10^{19}$	-1.20	0.055	$7.3 \times 10^{21}$	$2.4 \times 10^{20}$
Sk $-67^\circ 2$	$1.0 \times 10^{21}$	$8.9 \times 10^{20}$	-0.19	0.190	$5.3 \times 10^{21}$	$4.7 \times 10^{21}$
Sk $-68^\circ 26$	$3.5 \times 10^{21}$	$2.4 \times 10^{20}$	-0.92	0.181	$1.9 \times 10^{22}$	$1.3 \times 10^{21}$
Sk $-68^\circ 129$	$5.2 \times 10^{21}$	$1.1 \times 10^{20}$	-1.38	0.201	$2.6 \times 10^{22}$	$5.5 \times 10^{20}$
Sk $-68^\circ 140$	$5.5 \times 10^{21}$	$3.0 \times 10^{19}$	-1.97	0.215	$2.6 \times 10^{22}$	$1.4 \times 10^{20}$
Sk $-68^\circ 155$	$4.2 \times 10^{21}$	$9.8 \times 10^{19}$	-1.35	0.217	$1.9 \times 10^{22}$	$4.5 \times 10^{20}$
Sk $-69^\circ 228$	$4.0 \times 10^{21}$	$4.9 \times 10^{18}$	-2.61	0.145	$2.8 \times 10^{22}$	$3.4 \times 10^{19}$
Sk $-69^\circ 279^b$	$3.5 \times 10^{21}$	$2.0 \times 10^{20}$	-0.98	0.221	$1.6 \times 10^{22}$	$9.0 \times 10^{20}$
LMC: extinction pairs						
Sk $-66^\circ 19/\text{Sk } -69^\circ 83$	$7.0 \times 10^{21}$	$1.6 \times 10^{20}$	-1.64	0.25	$2.5 \times 10^{22}$	$6.4 \times 10^{20}$
Sk $-67^\circ 2/\text{Sk } -66^\circ 35$	$1.0 \times 10^{21}$	$8.9 \times 10^{20}$	-0.19	0.18	$5.6 \times 10^{21}$	$5.0 \times 10^{21}$
Sk $-68^\circ 26/\text{Sk } -66^\circ 35$	$3.5 \times 10^{21}$	$2.3 \times 10^{20}$	-0.94	0.19	$1.8 \times 10^{22}$	$1.2 \times 10^{21}$
Sk $-68^\circ 129/\text{Sk } -68^\circ 41$	$4.0 \times 10^{21}$	$1.1 \times 10^{20}$	-1.27	0.17	$2.3 \times 10^{22}$	$6.6 \times 10^{20}$

Table 7—Continued

Sight Line or Extinction Pair	$N(\text{H I})$ ( $\text{cm}^{-2}$ )	$N(\text{H}_2)$ ( $\text{cm}^{-2}$ )	$\log_{10}f_{\text{H}_2}$	$E'(B-V)^a$ (mag)	$N(\text{H I})/E'(B-V)$ ( $\text{cm}^{-2} \text{mag}^{-1}$ )	$N(\text{H}_2)/E'(B-V)$ ( $\text{cm}^{-2} \text{mag}^{-1}$ )
LMCAvg curve <sup>c</sup>	...	...	-1.00	...	$1.1 \times 10^{22}$	$5.9 \times 10^{20}$
Sk $-68^\circ 140$ /Sk $-68^\circ 41$	$4.0 \times 10^{21}$	$3.0 \times 10^{19}$	-1.83	0.20	$2.0 \times 10^{22}$	$1.5 \times 10^{20}$
Sk $-68^\circ 155$ /Sk $-67^\circ 168$	$5.0 \times 10^{21}$	$9.8 \times 10^{19}$	-1.42	0.20	$2.5 \times 10^{22}$	$4.9 \times 10^{20}$
Sk $-69^\circ 228$ /Sk $-65^\circ 15$	$3.5 \times 10^{21}$	$4.9 \times 10^{18}$	-2.56	0.15	$2.3 \times 10^{22}$	$3.3 \times 10^{19}$
Sk $-69^\circ 270$ /Sk $-67^\circ 78$	$3.5 \times 10^{21}$	$0.7 \times 10^{20}$	-1.69	0.19	$1.8 \times 10^{22}$	$3.7 \times 10^{20}$
Sk $-69^\circ 279$ /Sk $-65^\circ 63$	$4.0 \times 10^{21}$	$2.0 \times 10^{20}$	-1.04	0.21	$1.9 \times 10^{22}$	$9.7 \times 10^{20}$
LMC2 curve <sup>c</sup>	...	...	-1.50	...	$1.9 \times 10^{22}$	$3.1 \times 10^{20}$

<sup>a</sup>As defined in the text,  $E'(B-V)$  refers to the portion of  $E(B-V)$  for each star arising in the Magellanic Clouds; the value listed for each extinction pair is equivalent to the quantity  $\Delta(B-V)$  in Table 1.

<sup>b</sup>The atomic hydrogen column density for Sk  $-69^\circ 279$  is based on  $N(\text{H I})_{LMC}$  from nearby stars, since no previously-published measurement could be found.

<sup>c</sup>Gas-to-dust ratios for each of the two LMC group mean extinction curves are included. In order to derive representative molecular gas-to-dust ratios, an  $f(\text{H}_2)$ -value was assumed for each curve and compared with the atomic gas-to-dust ratio determined from our averaging code; the results of these calculations are roughly consistent with the sight line properties in each group.  $R_V$ -values determined for the LMCAvg and LMC2 mean

curves are  $3.49 \pm 0.17$  and  $3.24 \pm 0.13$ , respectively.

Note. — Comparison of our  $\text{H}_2$  measurements with Tumlinson et al. (2002) required estimates of  $N(\text{H I})_{LMC}$  and  $E'(B-V)$ , the Magellanic Cloud portion of the color excess; our sources are Fitzpatrick (1985a,b). The properties for extinction pairs studied by Gunderson, Clayton, & Green (1998), Sk -66°19 and Sk -69°270, are listed for comparison.

Table 8. MEM Curve Abundance Requirements

Extinction Grouping	Silicon AS	Carbon Total	AMC	Graphite
SMC Wing	170%	44%	15%	29%
SMC Bar	78%	19%	14%	5%
LMCAvg	45%	100%	77%	23%
LMC2	19%	78%	66%	12%
HD 14250	114%	75%	51%	24%

Note. — Our MEM modelling reproduced curves corresponding to the FM parameters fit to the average extinction curves for each sight line grouping including wavenumbers from 0.455 to 9.575  $\mu\text{m}^{-1}$ ; a typical Galactic sight line is represented here by HD 14250 ( $R_V=2.98\pm0.14$ ; Paper I). The demands on each element are expressed as a percentage of the total interstellar abundance for each of the astronomical silicate (AS), amorphous carbon (AMC), and graphite grain components.